Supporting Information

Chiroptical inversion of a planar chiral redox-switchable rotaxane

Marius Gaedke,[a] Felix Witte,[a] Jana Anhäuser,[b] Henrik Hupatz,[a] Hendrik V. Schröder,[a] Arto Valkonen,[c], Kari Rissanen,[c] Arne Lützen,[b] Beate Paulus[a] and Christoph A. Schalley*[a]

[a] Institut für Chemie und Biochemie, Organische Chemie, Freie Universität Berlin, Takustraße 3, 14195 Berlin, Germany.
[b] Kekulé-Institut für Organische Chemie und Biochemie, Universität Bonn, Gerhard-Domagk-Str. 1, 53121 Bonn, Germany.
[c] University of Jyvaskyla, Department of Chemistry, P.O. Box 35, 40014 Jyväskylä, Finland.
*Corresponding author e-mail: c.schalley@fu-berlin.de

Table of contents

1. Experimental details

1.1. General methods

All reagents and solvents were obtained from commercial sources and used without further purification. Dry solvents were purchased from Acros Organics or obtained from the M. BRAUN Solvent purification system SPS 800. 2-Hydroxyethyl 4-methylbenzenesulfonate **S4**,[1] 2-[(tetrahydropyran-2-yl)oxy]ethyl *p*-toluenesulfonate) **S5**,[2] 2,3-bis(2-cyanoethylthio)-6,7-bis(methylthio)tetrathiafulvalene **S12**,[3] axle **A1**,[4] and 2,6-dimethoxybenzonitrile oxide stopper **St1**[5] were synthesised according to literature procedures. Thin-layer chromatography was performed on silica gel-coated plates with fluorescent indicator F254 (Merck). For column chromatography, silica gel (0.04-0.063 mm, Merck) was used.

^{1}H and ^{13}C NMR experiments were performed on JEOL ECX 400, JEOL ECP 500, Bruker AVANCE 500 or Bruker AVANCE 700 instruments. Residual solvent signals were used as the internal standards. All shifts are reported in ppm and NMR multiplicities are abbreviated as s (singlet), d (doublet), t (triplet), m (multiplet) and br (broad). Coupling constants *J* are reported in Hertz. Compounds containing the tetrakis[3,5-bis(trifluoromethyl)phenyl]borate ($BArF_{24}^-$) anion show ^{13}C NMR spectra with ^{19}F, ^{10}B and ^{11}B couplings. These signals were denoted as one signal.

Melting points were determined on a SMP 30 (Stuart) instrument and are uncorrected.

High-resolution ESI mass spectra were measured on an Agilent 6210 ESI-TOF device. Tandem MS and infrared multiphoton dissociation (IRMPD) experiments were performed on a Varian Inc. Ionspec Q FT-7 equipped with a 7 T superconducting magnet and a Micromass Z-spray ESI source. HPLC grade solvents were used for sample preparation and the samples introduced into the ion source with a flow rate of 2-4 µL/min.

UV/Vis spectra were recorded with a Varian Cary 50 Bio spectrometer equipped with a xenon lamp. Solvents with HPLC grade and Suprasil glass cuvettes with a path-length of 1 cm were used.

ECD spectra were recorded on a JASCO-8-10 spectropolarimeter at 20°C. Solvents with HPLC grade and Suprasil glass cuvettes with a path-length of 2 mm were used. During the measurements, a constant flow of 3.2 L/min N_2 was provided. Each dataset is an average of three subsequent measurements.

CV measurements were carried out with an Autolab PGSTAT302N potentiostat in a 2 mL measuring cell in dichloromethane with 0.1 M n-Bu_4NPF_6 as the conducting salt. The working electrode was made of glassy carbon, the reference Ag electrode was etched with conc. aq. HCl. A Pt wire worked as a counter electrode. The cyclic voltammogram traces were recorded with 10, 25, 50, 100, 250, 500, 1000 and 2500 mV/s scan rates, to ensure that the observed

processes are reversible and diffusion-limited. For better comparability, only the 100 mV/s traces were plotted and compared in the discussion. In order to obtain the correct half-wave potentials, $FeCp^*/FeCp^{*+}$ was used as the reference. These values were afterwards referenced to Fc/Fc^+ as described in the literature.[6] The raw data was treated with Nova 1.5 by Metrohm and the plots were made with Origin *8* by OriginLab.

The chromatographic resolution was performed on a Shimadzu Prominence LC-20 HPLC system, equipped with two LC20-AT pumps, a DGU-20A3 solvent degasser, a diode array detector SPD-M20A (190-640 nm) and a fraction collector FRC-10A. For the analytical HPLC resolution, a Daicel CHIRALPAK® IA column (0.46 cm Ø, 25 cm) was used as the chiral stationary phase and *tert*-butyl methyl ether/CH_2Cl_2 (HPLC grade, 80:20 v/v) as the eluent with a flow rate of 1 mL/min. For the semi-preparative HPLC resolution, a CHIRALPAK® IA column (1 cm Ø, 25 cm) was used as the chiral stationary phase and *tert*-butyl methyl ether/dichloromethane (HPLC grade, 80:20 v/v) as the eluent with a flow rate of 4 mL/min.

1.2. Synthesis of dTTFC8

The directional wheel **dTTFC8** was synthesised starting from naphthalene-2,3-diol through consecutive substitution[7] with tetrahydropyranyl-protected mono- and pentaethylene glycol. After deprotection[8] to the diol and tosylation,[9] the corresponding diiodide was formed through a Finkelstein reaction.[4] In the last step, a CsOH•H_2O-mediated macrocyclisation[10] with the dicyanoethyl-protected TTF derivative[11] was carried out.

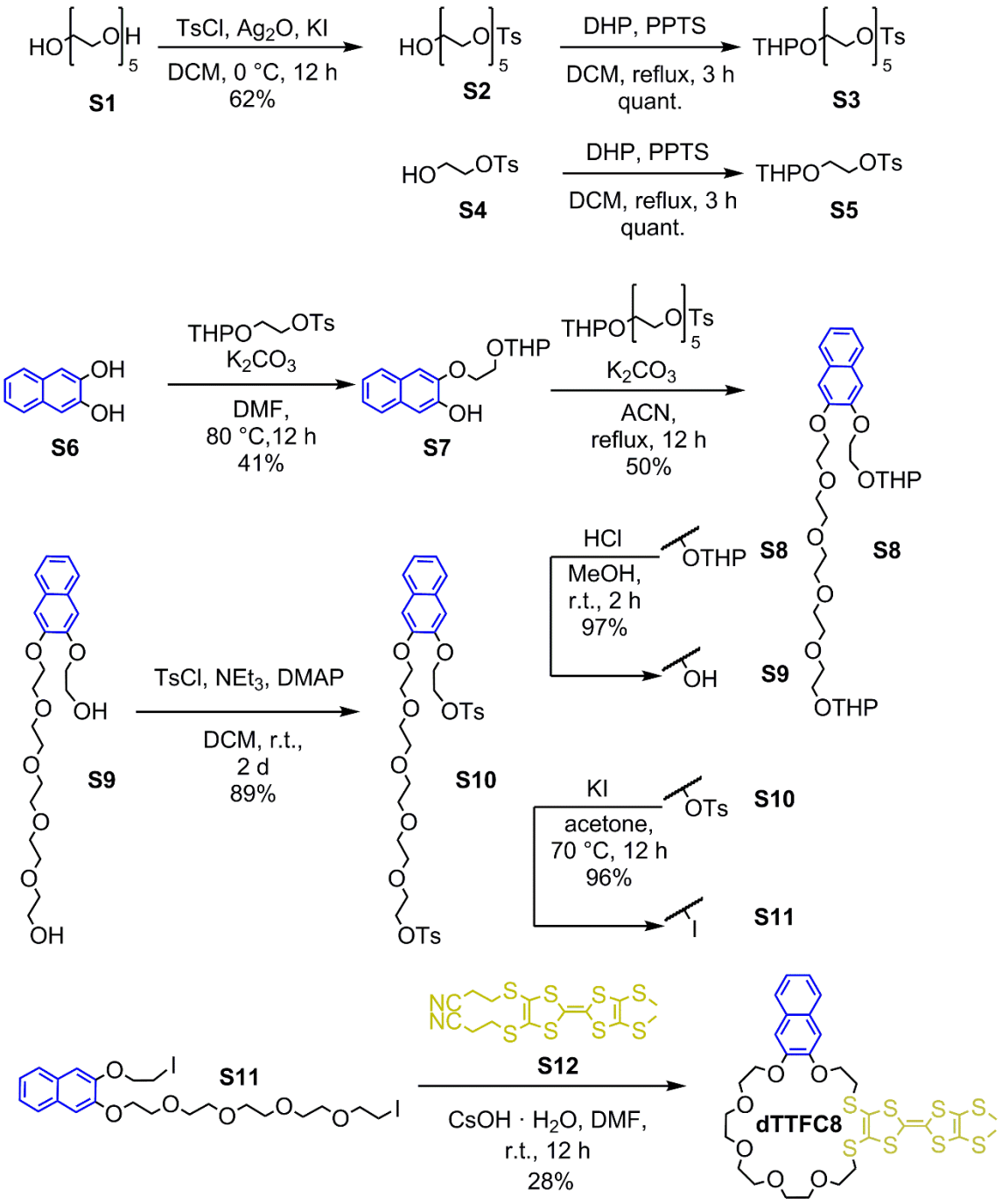

Scheme S1 Synthesis of wheel **dTTFC8** with a directional atom sequence.

14-Hydroxy-3,6,9,12-tetraoxatetradecyl 4-methylbenzenesulfonate[12]

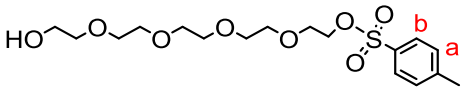

S2

4-Toluenesulfonyl chloride (444 mg, 2.3 mmol, 1.1 equiv.) was slowly added to a suspension of pentaethylene glycol **S1** (0.45 mL 1.9 mmol, 1.0 equiv.), KI (71.0 mg 0.42 mmol, 0.2 equiv.) and fresh Ag_2O (770 mg 3.3 mmol, 1.5 eq) in CH_2Cl_2 (21 mL) at 0 °C. The mixture was stirred overnight in a thawing ice bath. Afterwards, the mixture was filtered through a short celite pad and rinsed with EtOAc. After removal of the solvent, the crude product was purified by column chromatography (SiO_2, EtOAc/hexane = 2:1 → EtOAc, R_f ~ 0.3 in EtOAc) to isolate the desired product **S2** as a colourless oil in a 62% yield (466 mg, 1.2 mmol). **^{1}H NMR** (500 MHz, $CDCl_3$): δ = 2.42 (s, 3H, -C$\underline{H}_3$), 2.69 (s, 1H, -O$\underline{H}$), 3.47 – 3.70 (m, 18H, -OC$\underline{H}_2$), 4.08 – 4.17 (m, 2H, TsO-C$\underline{H}_2$-), 7.31 (d, J = 8.1 Hz, 2H, a), 7.76 (d, J = 8.1 Hz, 2H, b) ppm. **^{13}C NMR** (126 MHz, $CDCl_3$): δ = 21.7, 61.7, 68.7, 69.3, 70.3, 70.5, 70.6, 70.6, 70.6, 72.5, 128.0, 129.9, 133.0, 144.9 ppm. **ESI-HRMS**(ACN): *m/z* calcd. for [$C_{17}H_{28}O_8S$]: 415.1398 [M+Na]$^+$, found: 415.1394; calcd. for [M+K]$^+$:431.1137, found: 431.1130.

14-((Tetrahydro-2*H*-pyran-2-yl)oxy)-3,6,9,12-tetraoxatetradecyl 4-methylbenzenesulfonate[12]

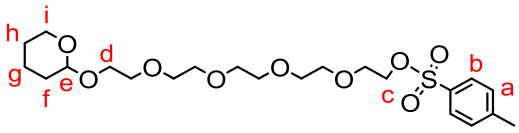

S3

A solution of monotosylate **S2** (1.00 g, 2.6 mmol, 1.0 equiv.), pyridinium tosylate (132 mg, 0.5 mmol, 0.2 equiv.) and 3,4-dihydro-*2H*-pyran (360 µL, 3.8 mmol, 97%, 1.5 equiv.) in CH_2Cl_2 (40 mL) was refluxed for 3 h. Afterwards, the mixture was poured into ice water, then extracted with CH_2Cl_2, washed with brine and dried with $MgSO_4$. After removal of the solvent, the crude product was purified by column chromatography (SiO_2, EtOAc, R_f ~ 0.6 in EtOAc) to isolate the desired product **S3** as a colourless oil in quantitative yield (1.26 g, 2.6 mmol). **^{1}H NMR** (500 MHz, $CDCl_3$): δ = 1.38 – 1.84 (m, 6H, f, g, h), 2.38 (s, 3H, -C$\underline{H}_3$), 3.38 – 3.49 (m, 2H, d), 3.49 – 3.65 (m, 16H, O-CH_2), 3.73 – 3.86 (m, 2H, i), 4.04 – 4.13 (m, 2H, c), 4.56 (dd, J = 4.3, 2.9 Hz, 1H, e), 7.29 (d, J = 8.1 Hz, 2H, a), 7.73 (d, J = 8.1 Hz, 2H, b) ppm. **^{13}C NMR:** (126 MHz, $CDCl_3$) δ = 19.4, 19.7, 21.6, 25.4, 30.5, 30.6, 43.6, 62.1, 62.8, 66.6, 68.6, 69.2, 70.4, 70.5, 70.6, 94.5, 94.5, 98.8, 98.9, 127.9, 129.8, 132.9 ppm. **ESI-HRMS**(ACN): *m/z* calcd. for [$C_{22}H_{36}O_9S$]: 499.1972 [M+Na]$^+$, found: 499.1955; calcd. for [M+K]$^+$: 515.1712, found: 515.1694.

3-(2-((Tetrahydro-2*H*-pyran-2-yl)oxy)ethoxy)-2-naphthol[7]

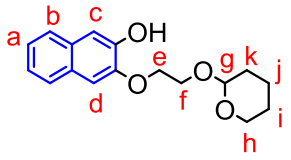

S7

A solution of protected monotosylate **S5** (96.0 mg, 0.32 mmol, 1.0 equiv.), naphthol **S6** (51.0 mg, 0.32 mmol, 1.0 equiv.) and K_2CO_3 (190 mg, 1.4 mmol, 4.3 eq) in dry DMF (20 mL) was stirred at 80 °C in an argon atmosphere for 12 h. Afterwards, residual K_2CO_3 was filtered off and the solvent was removed under reduced pressure. The crude product was then purified by column chromatography (SiO_2, CH_2Cl_2/MeOH = 100:1, R_f ~ 0.8 in CH_2Cl_2/MeOH = 50:1) to isolate the desired product **S7** as a colourless oil in a 41% yield (37.5 mg, 0.13 mmol). **^{1}H NMR** (500 MHz, $CDCl_3$): δ = 1.50 – 1.91 (m, 6H, j, k, l), 3.53 – 3.60 (m, 1H, h'), 3.89 – 3.97 (m, 2H, h'', f'), 4.07 – 4.16 (m, 1H,f''), 4.31 – 4.35 (m, 2H, e), 4.73 (dd, J = 4.6, 2.9 Hz, 1H, g), 7.20 (s, 1H, c), 7.27 (s, 1H, d), 7.28 – 7.34 (m, 2H, a, a'), 7.63 – 7.67 (m, 2H, b, b') ppm. **^{13}C NMR** (126 MHz, $CDCl_3$): δ = 19.7, 25.4, 30.7, 30.8, 62.8, 66.4, 69.5, 99.7, 109.0, 110.0, 123.5, 123.9, 124.6, 126.5, 126.7, 128.9, 130.4, 146.7, 147.0 ppm. **ESI-HRMS**(MeOH): *m/z* calcd. for $[C_{17}H_{20}O_4]$: 311.1254 $[M+Na]^+$, found: 311.1279; calcd for $[M+K]^+$ 327.0993, found: 327.1018.

2-(2-((3-((14-((Tetrahydro-2*H*-pyran-2-yl)oxy)-3,6,9,12-tetraoxatetradecyl)oxy)naphthalen-2-yl)oxy)ethoxy)tetrahydro-2*H*-pyran[7]

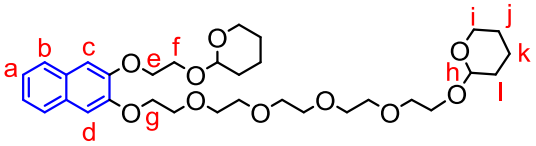

S8

A suspension of protected monotosylate **S3** (3.10 g, 6.44 mmol, 1 equiv.), monosubstituted naphthol **S7** (1.86 g, 6.44 mmol, 1 equiv.) and K_2CO_3 (3.80 g, 27.7 mmol, 4.3 equiv.) in dry ACN (100 mL) was refluxed under an argon atmosphere overnight. Afterwards K_2CO_3 was filtered off and the solvent was removed under reduced pressure. The crude product was then purified by column chromatography (SiO_2, EtOAc, R_f ~ 0.5 in EtOAc) to isolate the desired product **S8** as a colourless oil in a 50% yield (1.90 g, 3.21 mmol). **^{1}H NMR** (500 MHz, $CDCl_3$): δ = 1.44 – 1.90 (m, 12H, j, k, l), 3.45 – 3.61 (m, 4H, i), 3.61 – 3.91 (m, 15H, O-C$\underline{H}_2$), 3.91 – 3.96 (m, 2H, f), 3.96 – 4.02 (m, H, O-C$\underline{H}_2$), 4.11 – 4.16 (m, 1H, O-C$\underline{H}_2$), 4.17 – 4.23 (m, 1H, O-C$\underline{H}_2$), 4.25 – 4.33 (m, 4H, e, g), 4.59 – 4.63 (m, 1H, h), 4.73 – 4.78 (m, 1H, h'), 7.16 (s, 1H, d), 7.18 (s, 1H, c), 7.29 – 7.35 (m, 2H, a, a'), 7.63 – 7.67 (m, 2H, b, b') ppm. **^{13}C NMR** (126 MHz,

$CDCl_3$): δ = 19.4, 19.6, 19.9, 25.5, 25.6, 30.6, 30.7, 30.8, 62.2, 62.3, 65.7, 66.7, 68.3, 68. 6, 69.7, 70.6, 70.7, 70.7, 70.8, 71.1, 99.0, 108.7, 108.8, 124.3, 124.3, 124.5, 124.5, 126.4, 126.4, 126.5, 126.5, 129.4, 129.5, 129.6, 149.2, 149.3 ppm. **ESI-HRMS**(MeOH): *m/z* calcd. for [$C_{32}H_{48}O_{10}$]: 615.3140 [M+Na]$^+$, found: 615.3136; calcd for [M+K]$^+$: 631.2879, found: 631.2876.

14-((3-(2-Hydroxyethoxy)naphthalen-2-yl)oxy)-3,6,9,12-tetraoxatetradecan-1-ol[8]

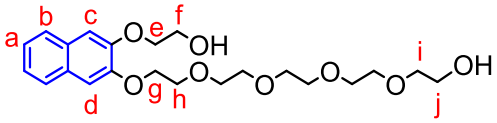

S9

A solution of diprotected glycol ether **S8** (1.90 g, 3.21 mmol) in MeOH (50 mL) was acidified with conc. HCl, until the solution reached pH = 1. After 2 h stirring at r.t. the solvent was removed under reduced pressure and the oily residue was stirred at 40 °C in oil pump vacuum for 5 h to obtain the desired product **S9** as a colourless oil in a 96% yield (1.31 g, 3.08 mmol). **^{1}H NMR** (500 MHz, $CDCl_3$): δ = 3.53 – 3.58 (m, 2H, j), 3.61 – 3.73 (m, 12H, O-C$\underline{H}_2$), 3.73 – 3.77 (m, 2H, i), 3.91 – 3.95 (m, 2H, h), 3.97 – 4.02 (m, 2H, f), 4.14 – 4.19 (m, 2H, e), 4.25 – 4.29 (m, 2H, g), 7.09 (s, 2H, d), 7.15 (s, 2H, c), 7.28 – 7.34 (m, 2H ,a, a'), 7.61 – 7.68 (m, 2H, b, b') ppm. **^{13}C NMR** (126 MHz, $CDCl_3$): δ = 60.9, 61.7, 68.2, 69.5, 70.3, 70.4, 70.6, 70.6, 70.7, 71.1, 72.7, 108.0, 108.1, 124.3, 124.5, 124.5, 126.4, 126.4, 129.2, 129.5, 148.7, 148.9 ppm. **ESI-HRMS**(ACN): *m/z* calcd. for [$C_{22}H_{32}O_8$]: 447.1989 [M+Na]$^+$, found: 447.1968; calcd for [M+K]$^+$: 463.1729, found: 463.1706.

2-((3-((14-(Tosyloxy)-3,6,9,12-tetraoxatetradecyl)oxy)naphthalen-2-yl)oxy)ethyl 4-methylbenzenesulfonate[9]

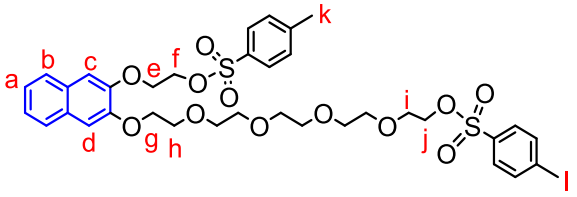

S10

A solution of 50 mg (0.12 mmol, 1.0 equiv.) diol **S9**, 100 µL (0.71 mmol, 6.0 eq) NEt_3, 0.1 mg (0.6 µmol, 0.5 mol%) DMAP and 135 mg (0.71 mmol, 6 eq) 4-toluenesulfonyl chloride in dry methylene chloride (25 mL) was left stirring at r.t. for 2 days. The reaction mixture was washed with saturated NH_4Cl aq. solution and dried with $MgSO_4$. The crude product was then purified by column chromatography (SiO_2, CH_2Cl_2 → EtOAc, R_f ~ 0.8 in EtOAc) to obtain the desired product **S10** as a colourless oil in 89% yield (77 mg, 0.11 mmol). **^{1}H NMR** (500 MHz, $CDCl_3$):

δ = 2.38 (s, 3H, l), 2.41 (s, 3H, k), 3.52 – 3.69 (m, 12H, O-CH_2), 3.75 – 3.78 (m, 2H, i), 3.91 – 3.95 (m, 2H, h), 4.11 – 4.15 (m, 2H, j), 4.22 – 4.26 (m, 2H, g), 4.27 – 4.32 (m, 2H, e), 4.41 – 4.47 (m, 2H, f), 7.04 (s, 1H, d), 7.14 (s, 1H, c), 7.27 – 7.36 (m, 6H, a, a', H-Ar-CCH_3), 7.58 – 7.67 (m, 2H, b, b'), 7.76 – 7.83 (m, 4H, H-Ar-CSO_3R) ppm. **^{13}C NMR** (126 MHz, $CDCl_3$): δ = 21.7, 21.7, 66.7, 68.2, 68.6, 68.7, 69.4, 69.6, 70.6, 70.6, 70.7, 70.8, 70.8, 71.0, 100.1, 108.9, 110.0, 110.0, 124.4, 124.7, 126.4, 126.5, 128.0, 128.1, 129.2, 129.9, 129.9, 129.9, 130.0, 133.0, 133.1, 144.9, 144.9, 145.0, 148.2, 149.1 ppm. **ESI-HRMS**(ACN): *m/z* calcd. for [$C_{36}H_{44}O_{12}S_2$]: 755.2166 [M+Na]$^+$, found: 755.2168; calcd for [M+K]$^+$: 771.1906, found: 771.1905.

1-Iodo-14-((3-(2-iodoethoxy)naphthalen-2-yl)oxy)-3,6,9,12-tetraoxatetradecane[4]

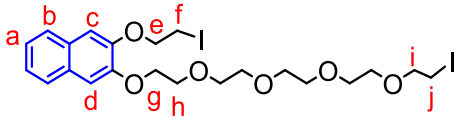

S11

A solution of 61.4 mg (83.8 µmol, 1.0 eq) ditosylate **S10** and 55.6 mg (335 mmol, 4.0 eq) KI in acetone (5 mL) was stirred at 70 °C overnight. When the reaction mixture turned yellow and a white precipitate formed, the solvent was removed under reduced pressure. The residue was dissolved in EtOAc and washed with brine. After drying with $MgSO_4$, the solvent was removed to isolate the desired product **S11** as a yellowish oil in a 96% yield (52 mg, 80.9 µmol). **^{1}H NMR** (500 MHz, $CDCl_3$): δ = 3.21 – 3.25 (m, 2H, j), 3.49 – 3.53 (m, 2H, f), 3.61 – 3.71 (m, 10H, O-CH_2), 3.71 – 3.74 (m, 2H, i), 3.78 – 3.82 (m, 2H, O-CH_2), 3.94 – 3.97 (m, 2H, h), 4.26 – 4.30 (m, 2H, g), 4.35 – 4.40 (m, 2H, e), 7.15 (s, 1H, d), 7.18 (s, 1H, c), 7.31 – 7.34 (m, 2H, a, a'), 7.64 – 7.67 (m, 2H, b, b') ppm. **^{13}C NMR** (126 MHz, $CDCl_3$): δ = 68.8, 69.7, 69.9, 70.3, 70.3, 70.7, 70.7, 70.8, 70.8, 71.1, 72.1, 72.1, 109.0, 109.9, 124.5, 124.7, 126.5, 126.5, 129.3, 129.8, 148.1, 149.1 ppm. **ESI-HRMS**(ACN): *m/z* calcd. for [$C_{22}H_{30}I_2O_6$]: 667.0024 [M+Na]$^+$, found: 666.9996; calcd. for [M+K]$^+$: 682.9763, found: 682.9730.

2-(4,5-Bis(methylthio)-1,3-dithiol-2-ylidene)-5,6,8,9,11,12,14,15,17,18,27,28-dodeca-hydro-[1,3]dithiolo[4,5-t]naphtho[2,3-b][1,4,7,10,13,16]hexaoxa[19,22]dithiacyclo-tetracosane[10]

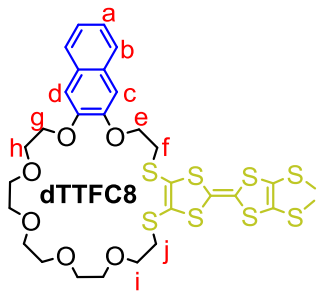

A solution of 74 mg (0.44 mmol, 2.0 equiv.) CsOH · H_2O in dry MeOH (2 mL) was added over 30 min to 104 mg (0.22 mmol, 1.0 equiv.) TTF precursor **S12** in dry DMF (5 mL). After the mixture turned dark red, it was added over 1 h to 143 mg (0.22 mmol, 1.0 equiv.) to diiodide **S11** in dry DMF (25 mL) and stirred at r.t. under argon overnight. Afterwards, the solvent was removed under reduced pressure and the residue was dissolved in CH_2Cl_2. The solution was washed with water and brine. After drying with $MgSO_4$, the crude product was purified by column chromatography (SiO_2, CH_2Cl_2, R_f ~ 0.5 in CH_2Cl_2/MeOH = 100:1) to isolate the desired product **dTTFC8** as an orange powder in a 28% yield (45.7 mg, 61 µmol). **M.p.** 79.3°C; **^{1}H NMR** (700 MHz, CD_2Cl_2): δ = 2.43 (s_{br}, 6H, S-CH_3), 3.02 (s_{br}, 4H, j), 3.30 (t, J = 6.5 Hz, 2H, f), 3.49 – 3.52 (m, 2H, O-C$\underline{H}_2$), 3.53 – 3.56 (m, 2H, O-C$\underline{H}_2$), 3.56 – 3.59 (m, 2H, O-C$\underline{H}_2$), 3.59 – 3.65 (m, 4H, i, O-C$\underline{H}_2$), 3.65 – 3.68 (m, 2H, O-C$\underline{H}_2$), 3.76 – 3.79 (m, 2H, O-C$\underline{H}_2$), 3.89 – 3.97 (m, 2H, h), 4.25 (m, 2H, O-C$\underline{H}_2$), 4.38 (s_{br}, 2H, e), 7.17 (s, 1H, c), 7.20 (s, 1H, d), 7.30 – 7.35 (m, 2H, a), 7.66 – 7.70 (m, 2H, b).ppm. **^{13}C NMR** (176 MHz, CD_2Cl_2): δ = 23.3, 29.9, 30.3, 32.5, 68.4, 69.5, 70.0, 71.0, 71.1, 71.2, 71.3, 71.7, 109.1, 109.8, 124.8, 124.9, 126.8, 126.9, 129.8, 130.2, 149.1, 149.7 ppm. **ESI-HRMS**(ACN): *m/z* calcd. for [$C_{30}H_{36}O_6S_8$]: 771.0170 [M+Na]$^+$, found: 771.0182; calcd. for [M+K]$^+$: 786.9909, found: 786.9916.

1.3. Synthesis of [2]rotaxane (*rac*)-2 and (*rac*)-2Ac

[2]Rotaxane (*rac*)-2

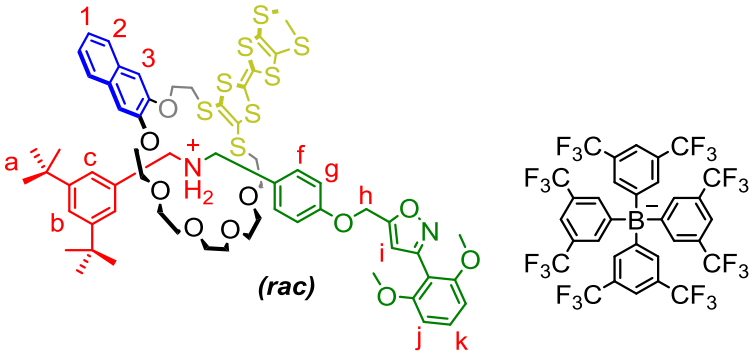

(*rac*)-**2**

Axle **A1** (74 mg, 60 µmol, 1.0 equiv.) and macrocycle **dTTFC8** (50 mg, 67 µmol, 1.1 equiv.) were dissolved in dry CH_2Cl_2 (200 µL) and stirred at r.t. for 10 min. Afterwards 2,6-dimethoxybenzonitrile oxide **St1** (14 mg, 78 µmol, 1.3 equiv.) was added and the mixture was stirred in a sealed tube under argon at 35 °C overnight. Then, the mixture was applied directly onto a preparative thin layer chromatography plate (SiO_2 2000 µm, CH_2Cl_2, R_f ~ 0.6 in CH_2Cl_2) to obtain the desired racemic product (*rac*)-**2** (129 mg, 60 µmol, 73 %) as a yellowish oil. **^{1}H NMR** (700 MHz, CD_2Cl_2): δ = 1.25 (s, 18H, a), 2.42 (s, 3H, -SMe), 2.43 (s, 3H, -SMe), 3.05 – 3.18 (m, 6H, O-C$\underline{H}_2$), 3.23 – 3.33 (m, 4H, O-C$\underline{H}_2$), 3.37 – 3.46 (m, 4H, O-C$\underline{H}_2$), 3.58 – 3.68 (m, 2H, O-C$\underline{H}_2$), 3.75 – 3.91 (m, 10H, O-C$\underline{H}_2$, -OMe), 4.28 – 4.40 (m, 2H, O-C$\underline{H}_2$), 4.43 – 4.46 (m, 2H, O-C$\underline{H}_2$), 4.53 – 4.77 (m, 4H, C$\underline{H}_2$-NH_2), 5.04 (d, *J* = 12.8 Hz, 1H, h), 5.08 (d, *J* = 13.0 Hz, 1H, h), 6.44 (s, 1H, i), 6.66 (d, *J* = 8.5 Hz, 2H, j), 6.95 (d, *J* = 8.7 Hz, 2H, g), 7.19 (s, 1H, 3), 7.24 (s, 1H, 3), 7.27 (d, *J* = 1.6 Hz, 2H, c), 7.35 – 7.41 (m, 5H, f, k, 1), 7.47 (t, *J* = 1.8 Hz, 1H, b), 7.55 (s_{br}, 4H, $BArF_{24}$), 7.66 – 7.69 (m, 2H, 2), 7.69 (s_{br}, 8H, $BArF_{24}$) 7.77 – 7.86 (m, 2H, NH_2) ppm. **^{13}C NMR** (176 MHz, CD_2Cl_2): δ = 19.6, 31.7, 35.4, 36.3, 37.3, 53.3, 56.5, 61.6, 68.7, 69.4, 70.5, 70.6, 71.0, 71.2, 71.2, 71.3, 71.5, 104.7, 107.3, 107.4, 109.1, 109.3, 109.6, 113.8, 115.6, 118.0, 118.1, 124.4, 124.7, 124.8, 125.0, 125.7, 126.0, 126.9 127.5, 127.8, 128.2, 128.2, 128.8, 129.4, 129.8, 129.9, 130.9, 132.0, 132.0, 135.4, 148.3, 148.4, 152.4, 157.8, 159.5, 162.3, 166.2 ppm. **ESI-HRMS**(MeOH): *m/z* calcd. for $[C_{64}H_{79}N_2O_{10}S_8]^+$: 1291.3495 $[M]^+$, found: 1291.3479.

[2]Rotaxane (*rac*)-2Ac

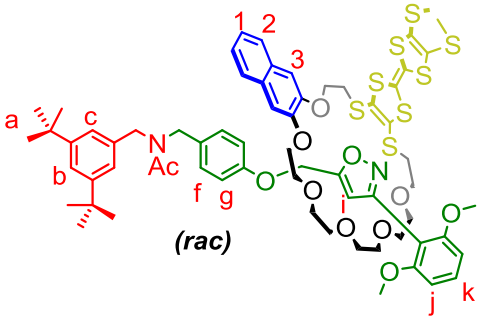

(*rac*)-**2Ac**

Rotaxane (*rac*)-**2** (14 mg, 6.5 µmol, 1.0 equiv.), NEt_3 (27 µL, 190 µmol, 30.0 equiv.) and Ac_2O (18 µL, 190 µmol, 30.0 equiv.) were dissolved in ACN (5 mL) and stirred at r.t. overnight. Then, the crude mixture was purified by preparative TLC (SiO_2 2000 µm, CH_2Cl_2/MeOH 50:1, R_f ~ 0.3 in CH_2Cl_2/MeOH = 50:1) to isolate the desired racemic product (*rac*)-**2Ac** as a yellowish oil in 95% yield (8.2 mg, 3.5 µmol). **^{1}H NMR** (700 MHz, CD_2Cl_2): δ = 1.29 (s, 9H, a), 1.32 (s, 9H, a), 1.78 (s, 1.5H, Ac), 1.90 (s, 1.5H, Ac), 2.24 (s, 1.5H, SMe), 2.30 (s, 1.5H, SMe), 2.33 (s, 1.5H, SMe), 2.34 (s, 1.5H, SMe), 3.02 – 3.15 (m, 3.6H, O-CH_2), 3.16 – 3.22 (m, 1.4H, O-CH_2), 3.34 – 3.44 (m, 4.5H, O-CH_2), 3.45 – 3.62 (m, 8H, O-CH_2), 3.64 – 3.74 (m, 5H, O-CH_2), 3.78 (d, *J* = 3.9 Hz, 6H, OMe), 3.81 – 3.83 (m, 0.7H, O-CH_2), 3.83 – 3.85 (m, 0.7H, O-CH_2), 3.95 – 4.04 (m, 4H, CH_2-N, O-CH_2), 4.05 – 4.13 (m, 2H, O-CH_2), 4.18 – 4.21 (m, 1H, CH_2-N), 4.22 – 4.26 (m, 1H, O-CH_2), 4.29 – 4.32 (m, 1H, CH_2-N), 4.37 – 4.40 (m, 1H, CH_2-N), 4.41 – 4.46 (m, 1H, CH_2-N), 5.80 – 5.87 (m, 2H, h), 6.64 (dd, *J* = 8.4, 5.6 Hz, 2H, j), 6.71 – 6.73 (m, 2H, g, i), 6.78 – 6.81 (m, 1H, g), 6.85 (s, 0.5H, 3), 6.87 (d, *J* = 1.8 Hz, 1H, c), 6.90 (s, 0.5H, 3), 6.91 (d, *J* = 1.8 Hz, 1H, c), 7.00 – 7.02 (m, 2H, f), 7.05 (*s*, 0.5H, 3), 7.07 (*s*, 0.5H, 3), 7.19 – 7.25 (m, 2H, 1), 7.29 (t, *J* = 1.9 Hz, 0.5H, b), 7.33 (t, *J* = 1.8 Hz, 0.5H, b), 7.35 (td, *J* = 8.4, 4.6 Hz, 1H, k), 7.55 – 7.59 (m, 1H, 2), 7.60 – 7.64 (m, 1H, 2) ppm. **^{13}C NMR** (176 MHz, CD_2Cl_2): δ = 19.2, 19.3, 19.3, 19.4, 21.8, 21.8, 30.3, 31.8, 32.5, 34.6, 35.2, 35.3, 35.5, 35.6, 46.59, 47.9, 48.8, 50.9, 51.3, 56.5, 56.5, 61.4, 61.4, 67.5, 67.5, 69.1, 69.2, 70.1, 70.2, 70.2, 70.5, 70.5, 71.2, 71.3, 71.3, 71.5, 71.5, 71.7, 71.7, 71.9, 104.5, 104.6, 107.1, 107.4, 107.5, 108.0, 108.1, 108.4, 108.4, 110.0, 110.1, 110.8, 115.2, 115.4, 121.0, 121.6, 121.8, 122.4, 123.9, 124.3, 124.6, 124.6, 124.6, 126.6, 126.7, 126.7, 126.7, 127.6, 127.7, 128.8, 129.0, 129.5, 129.6, 129.6, 129.9, 131.5, 131.5, 134.2, 134.5, 136.7, 137.3, 148.8, 148.9, 149.0, 149.1, 151.9, 157.4, 158.2, 158.3, 159.3, 168.9, 169.1, 171.1, 171.2 ppm. **ESI-HRMS**(MeOH): *m/z* calcd. for [$C_{66}H_{80}N_2O_{11}S_8$]: 1333.3606 [M+H]$^+$, found: 1333.3505; calcd. for [M+Na]$^+$: 1355.3425, found: 1355.3442; calcd. for [M+K]$^+$: 1371.3165, found: 1371.3185.

2. FTICR mass spectroscopy

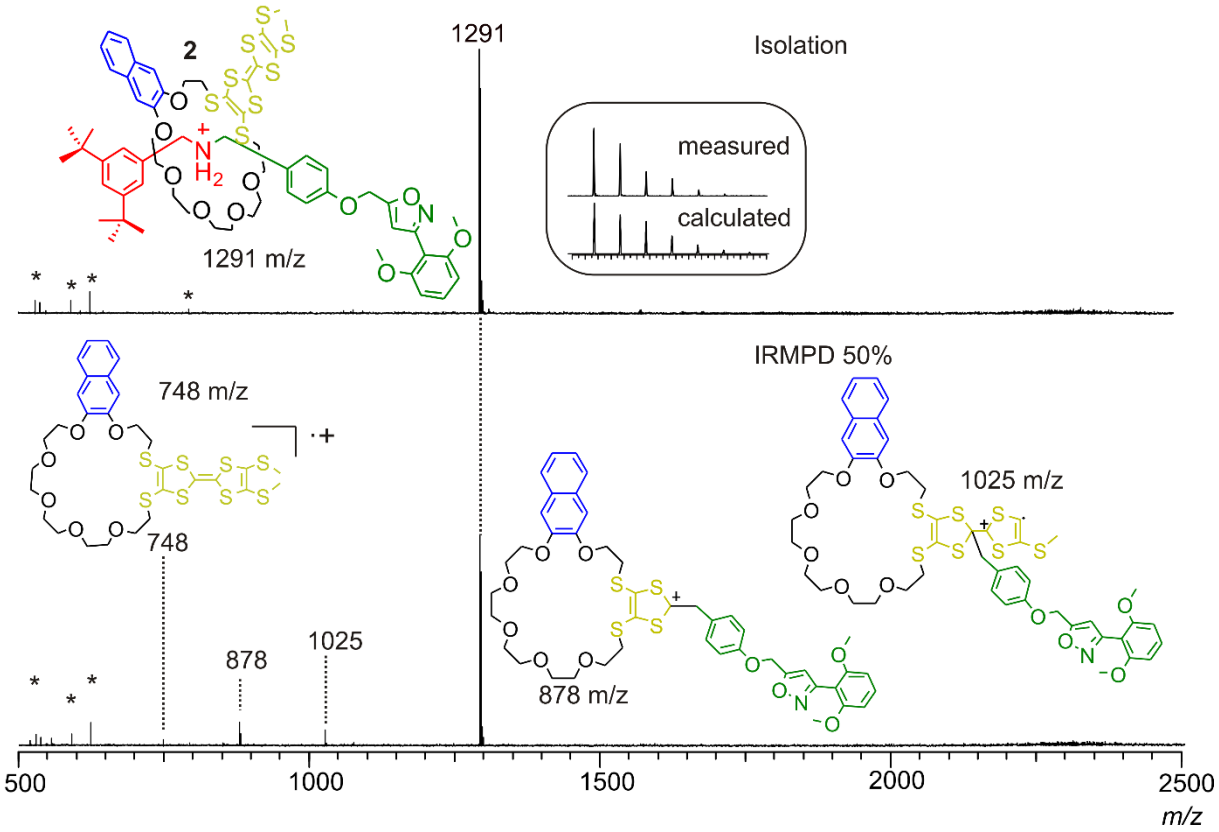

Fig. S1 ESI-FTICR infrared multiphoton dissociation (IRMPD) experiment with mass-selected rotaxane ions at *m/z* 1291 obtained from a MeOH solution (10 µM) of [2]rotaxane (*rac*)-**2**: (top) after mass-selection; (bottom) after fragmentation. The fragment peaks could be assigned to the free macrocycle as a radical cation (748 *m/z*) and two adducts, which arise from an attack of the TTF moiety on the benzylic position next to the nitrogen of the axle. These fragments are in line with the fragments obtained from rotaxanes of the non-directional **TTFC8** macrocycle.[4] As no free axle is observed as the fragmentation product, it can be concluded that the ionised and mass selected species are in fact mechanically interlocked. Electromagnetic stray radiation is marked with asterisks.

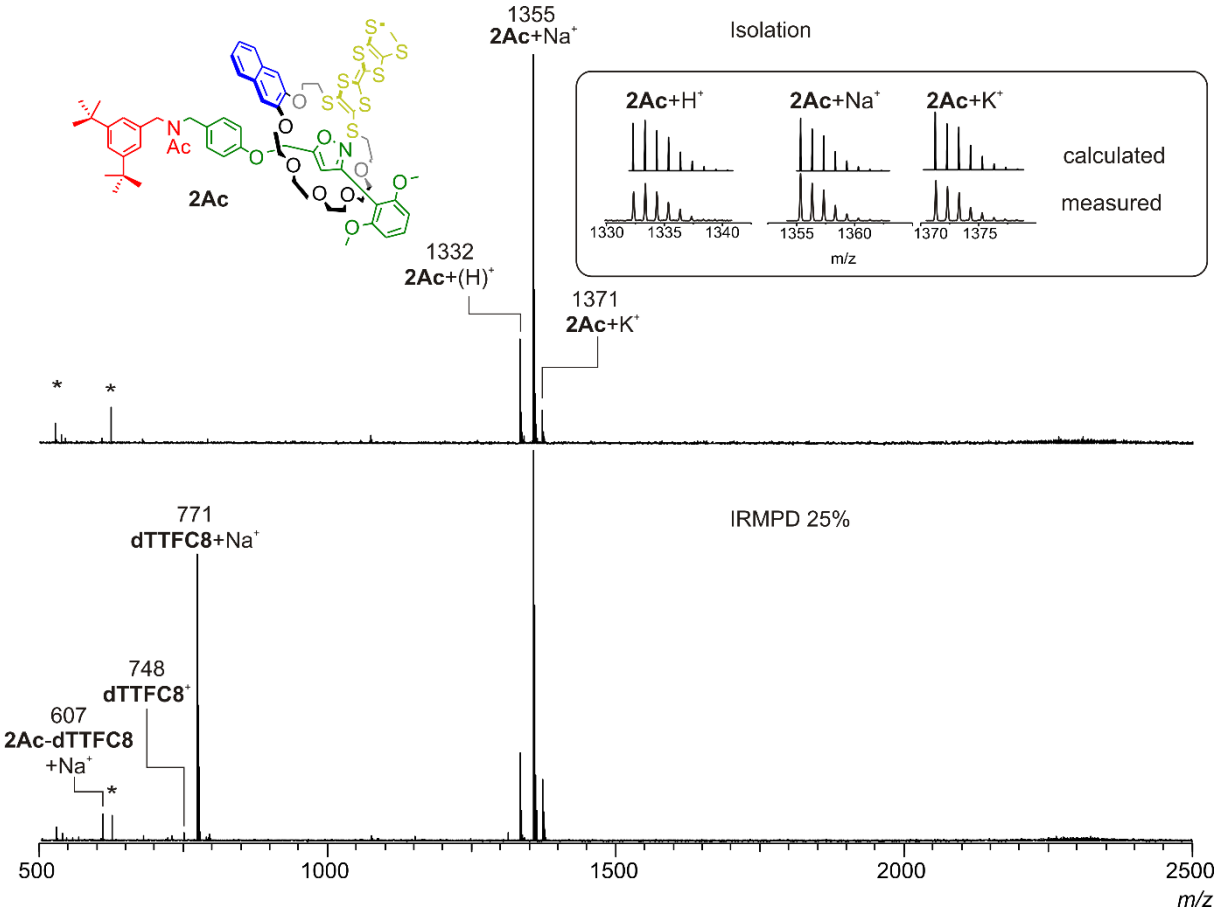

Fig. S2 ESI-FTICR infrared multiphoton dissociation (IRMPD) experiment with mass range-selected rotaxane ions obtained from a MeOH solution (10 µM) of [2]rotaxane (*rac*)-**2Ac**. The acetylated [2]rotaxane **2Ac** ions do not show the same fragmentation pattern as **2,** as no fragments from an intramolecular attack could be observed. Fragmentation proceeds by either losing the macrocycle (607 m/z) or fragmenting the axle leaving the charge on the macrocycle (748 and 771 m/z)

3. Variable Temperature NMR Spectroscopy

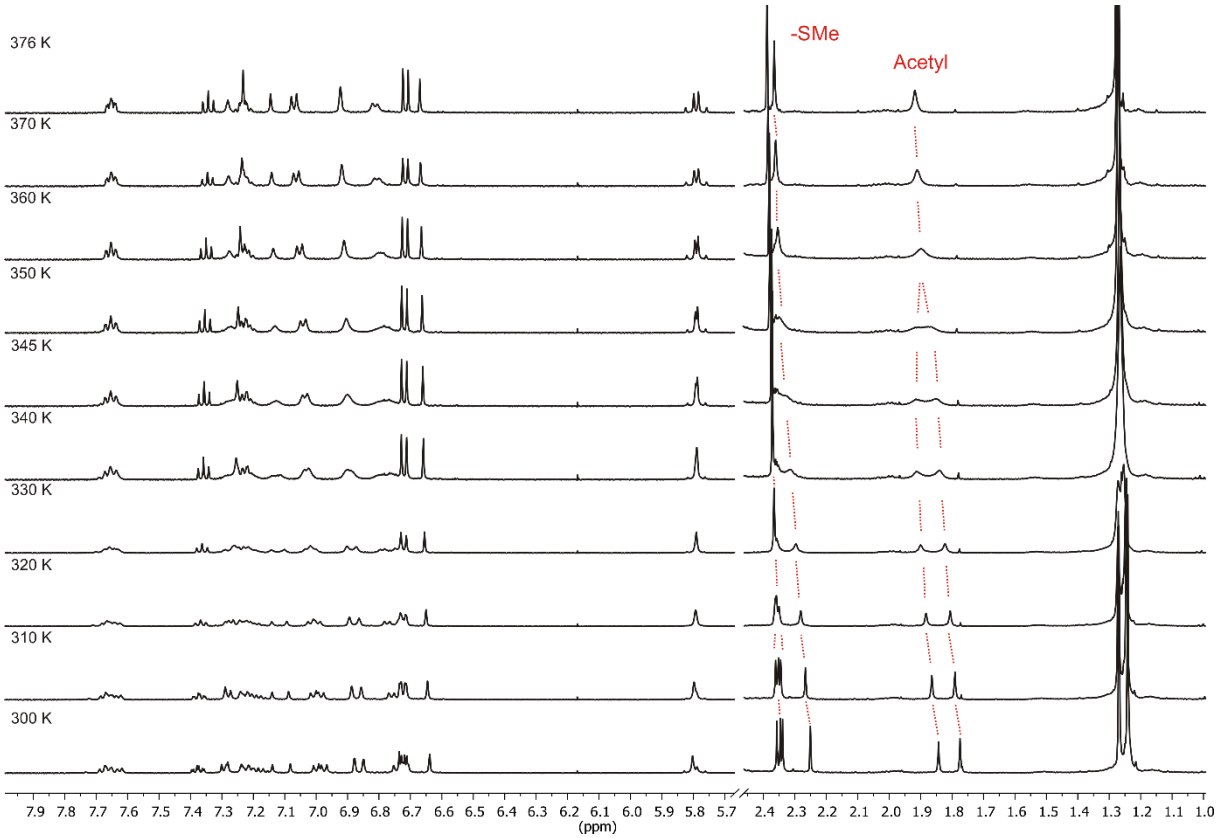

Fig. S3 Partial spectra of [2]rotaxane (*rac*)-**2Ac** in a VT ^{1}H NMR (500 MHz, DMSO-d6) experiment (gradual heating from 300 to 375 K), showing the coalescence of the acetyl groups and merging of the four singlets corresponding to SMe on the TTF into two singlets upon heating.

The free energy of activation ($\Delta G^{\ddagger}$) was calculated using the modified Eyring equation (eq. 1), where R is the ideal gas constant, T_c the coalescence temperature and $\Delta\nu$ the peak to peak separation between the signals for the two interconverting isomers in Hz.

$$\Delta G^{\ddagger} = R\,T_c\,(22.96 + \ln(T_c/\Delta\nu))\ \text{kJ mol}^{-1} \qquad \text{(eq. 1)}$$

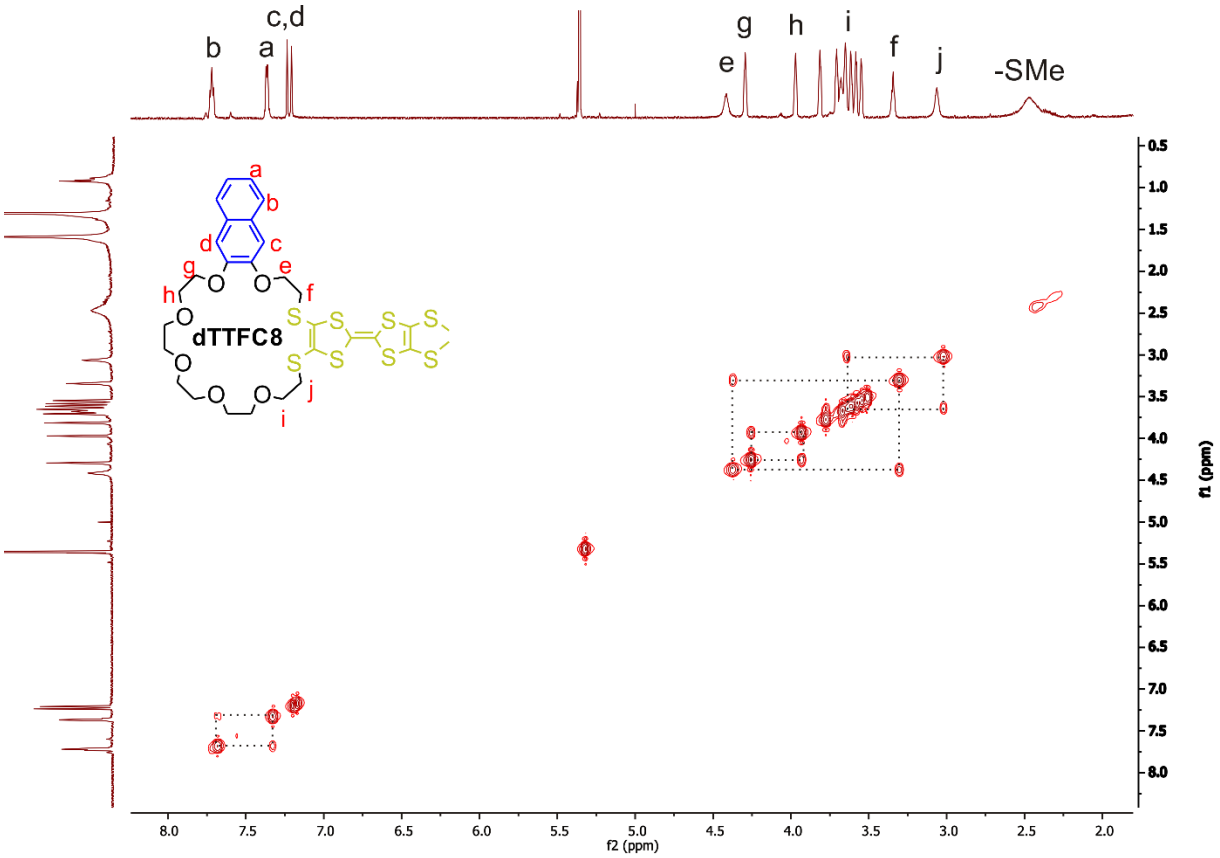

Fig. S4 COSY spectrum of **dTTFC8** in a (700 MHz, CD_2Cl_2).

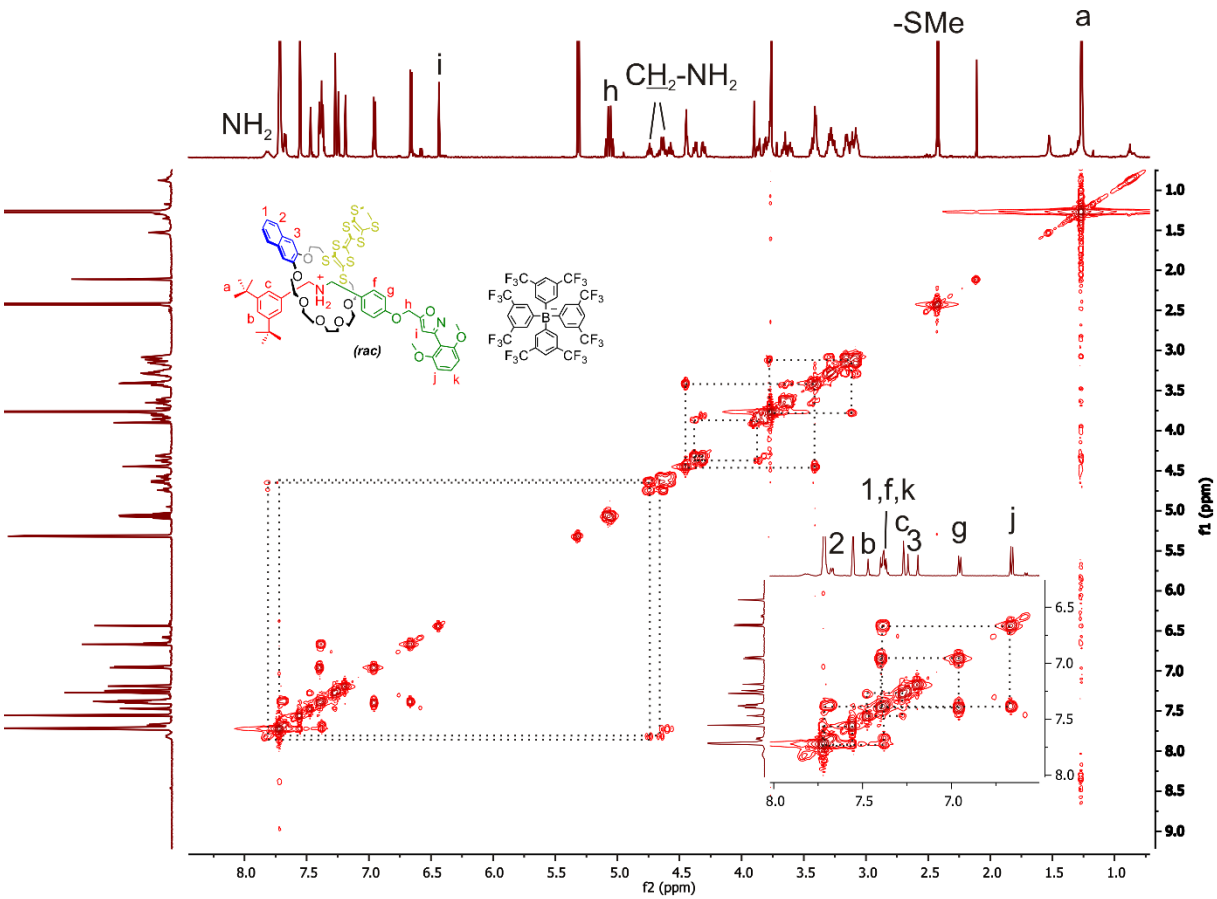

Fig. S5 COSY spectrum of (*rac*)-**2** in a (700 MHz, CD_2Cl_2).

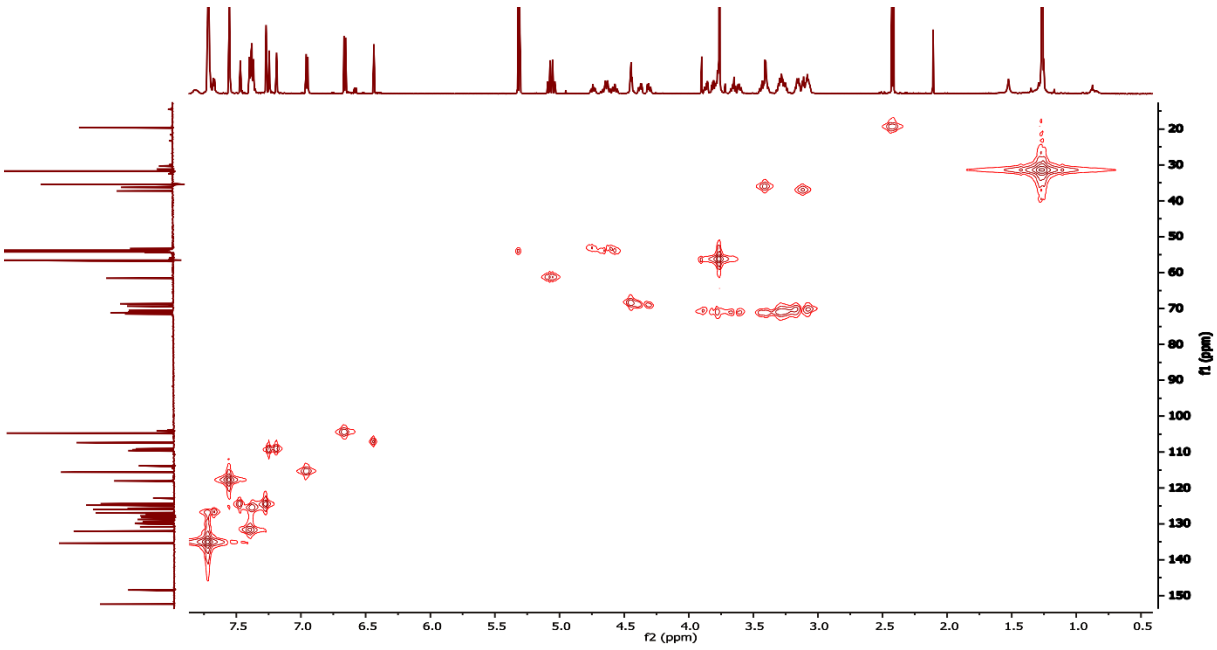

Fig. S6 HMQC spectrum of (*rac*)-**2** in a (700 MHz, CD_2Cl_2).

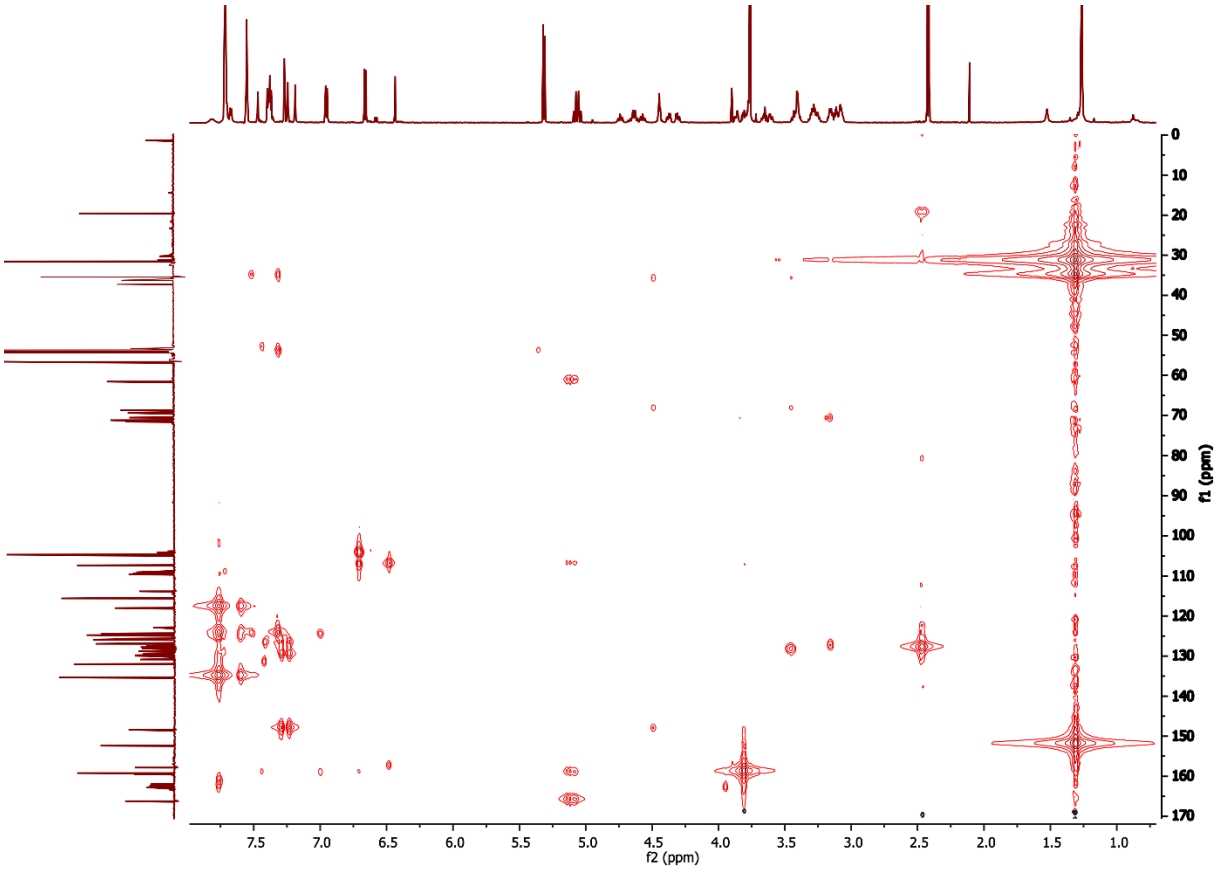

Fig. S7 HMBC spectrum of (*rac*)-**2** in a (700 MHz, CD_2Cl_2).

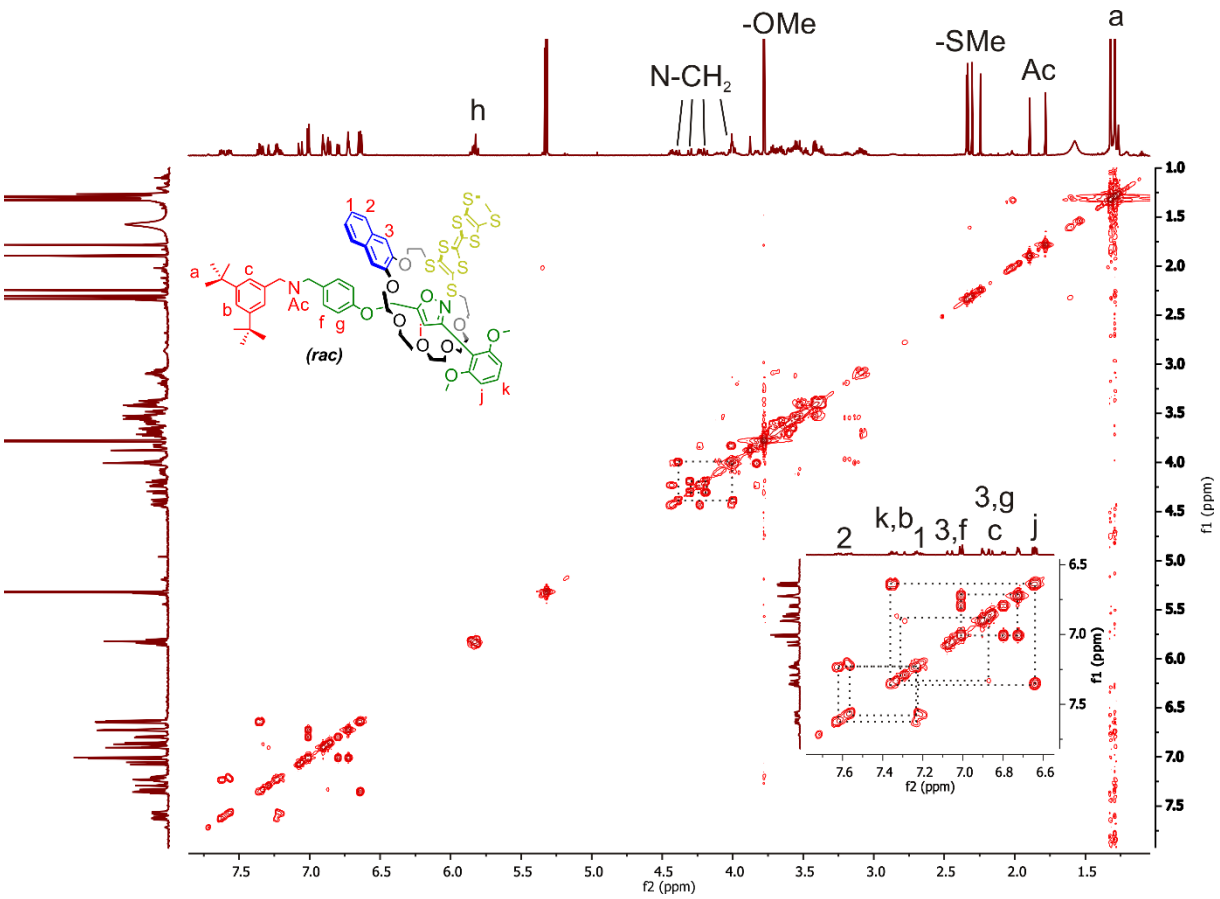

Fig. S8 COSY spectrum of (*rac*)-**2Ac** in a (700 MHz, CD_2Cl_2).

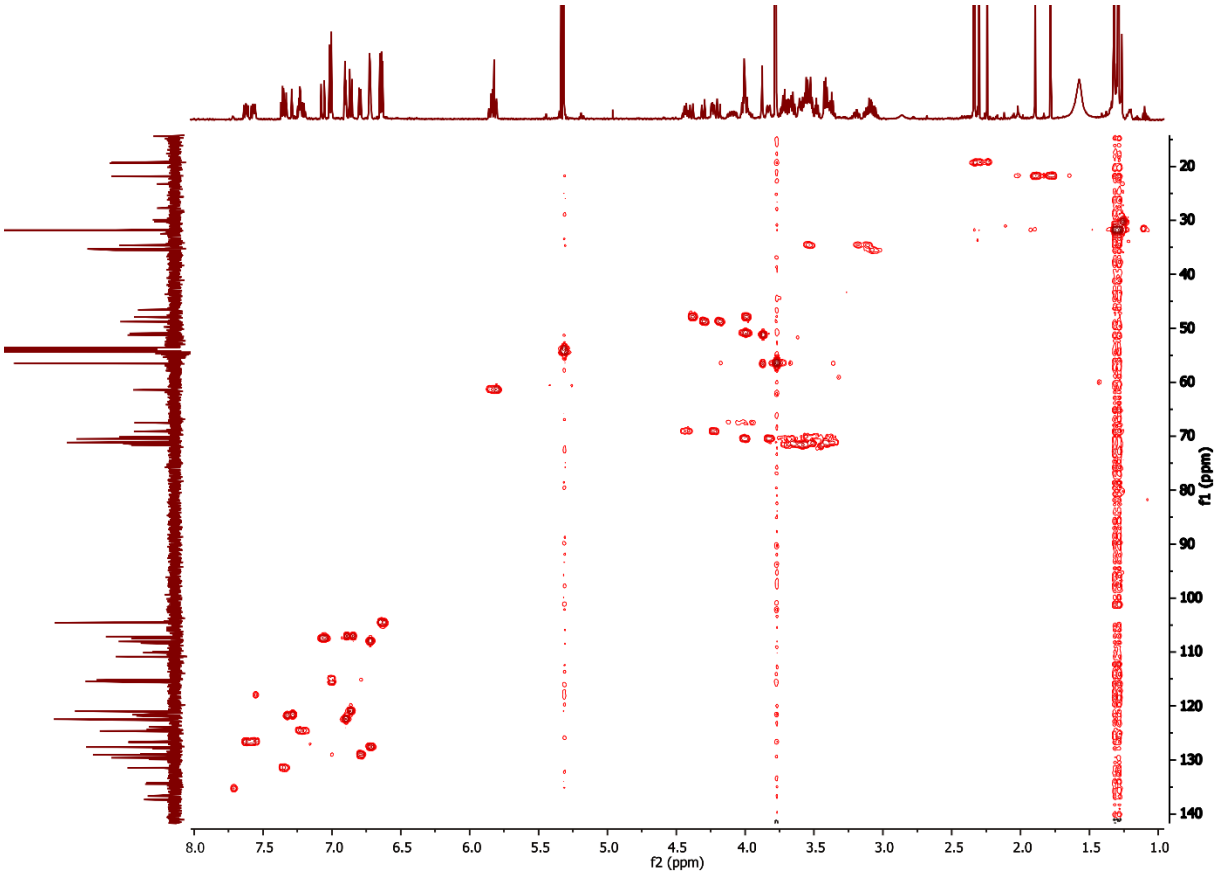

Fig. S9 HMQC spectrum of (*rac*)-**2Ac** in a (700 MHz, CD_2Cl_2).

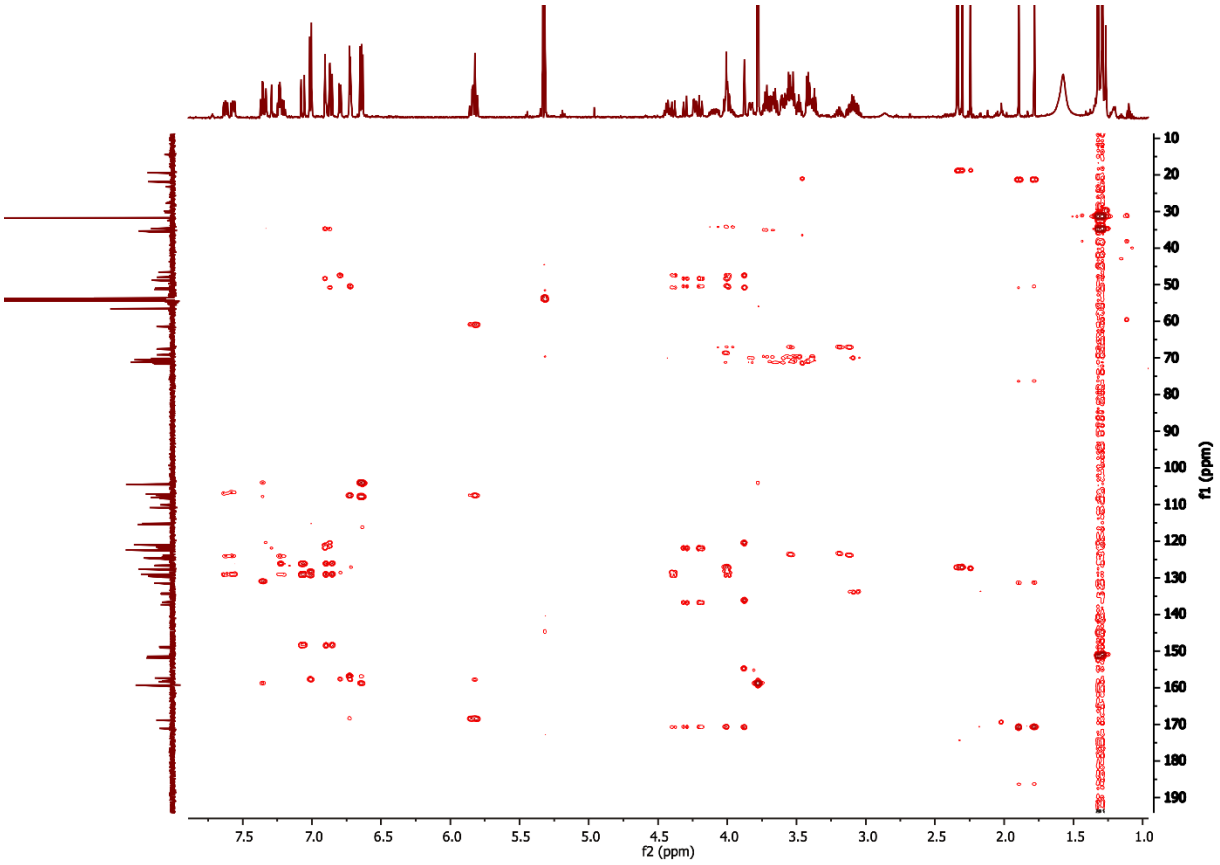

Fig. S10 HMBC spectrum of (*rac*)-**2Ac** in a (700 MHz, CD_2Cl_2).

4. Isothermal titration calorimetry

ITC experiments were carried out in dry 1,2-dichloroethane at 298 K on a TAM III microcalorimeter (Waters GmbH, TA Instruments, Eschborn, Germany). In a typical experiment, an 800 µL solution of crown ether was placed in the sample cell at a concentration of 1.1 mM, and 250 µL of a solution of the ammonium salt (8.0 mM) were put into the syringe. The titrations consisted of 32 consecutive injections of 8 µL each with a 15 min interval between injections. Heats of dilution were determined by titration of ammonium salt solutions into the sample cell containing blank solvent and were subtracted from each data set. The heat flow generated in the sample cell is measured as a differential signal between sample and reference cell. Hence, an exothermic event results in a positive and an endothermic in a negative heat flow. The data were analysed using the instrument's internal software package and fitted with a 1:1 binding model. Each titration was conducted three times and the measured values for *K* and Δ*H* were averaged.

Tab. S1: Thermodynamic data obtained from the ITC experiments.

	K_a /10^5 M^{-1}	ΔG / kJ mol^{-1}	ΔH / kJ mol^{-1}	$T\Delta S$ / kJ mol^{-1}
axle **A1⊂TTFC8**	4.4 ± 0,4	-32.2 ± 0.3	-46.2 ± 0.7	-14.0 ± 1.0
axle **A1⊂dTTFC8**	3.6 ± 0.3	-31.7 ± 0.2	-41.1 ± 1.1	-11.0 ± 1.3

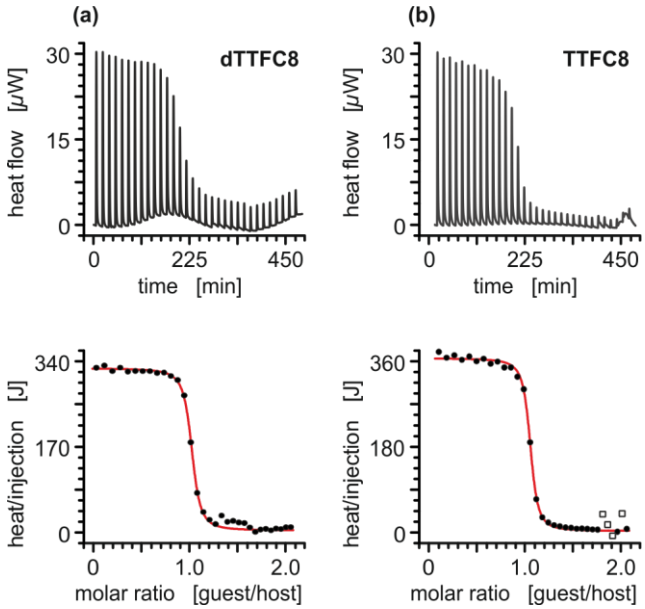

Figure S11. Titration plots (heat flow versus time and heat/volume versus guest/host ratio) obtained from ITC experiments at 298 K in 1,2-dichloroethane**: (a)** vial: **dTTFC8**, syringe: axle **A1**; **(b)** vial: **TTFC8**, syringe: axle **A1**; Points marked with non-filled squares were not considered in the fitting process.

5. Electrochemical measurements

Redox-potentials reported in this study were obtained by cyclic voltammetry. All measurements were at least conducted twice. Measurements were conducted in CH_2Cl_2 with 0.1 M electrolyte and 1 mM analyte concentration.

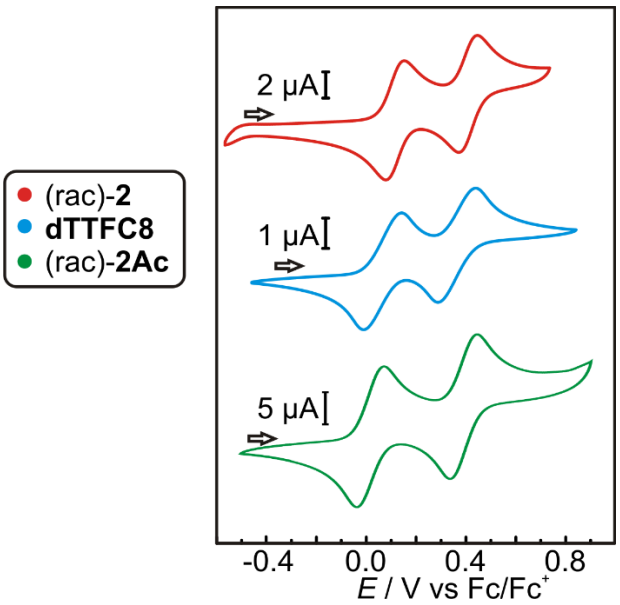

Fig. S12 Stacked cyclic voltammograms (CH_2Cl_2, n-Bu_4NPF_6, 298 K) of (*rac*)-**2**, **dTTFC8** and (*rac*)-**2Ac**

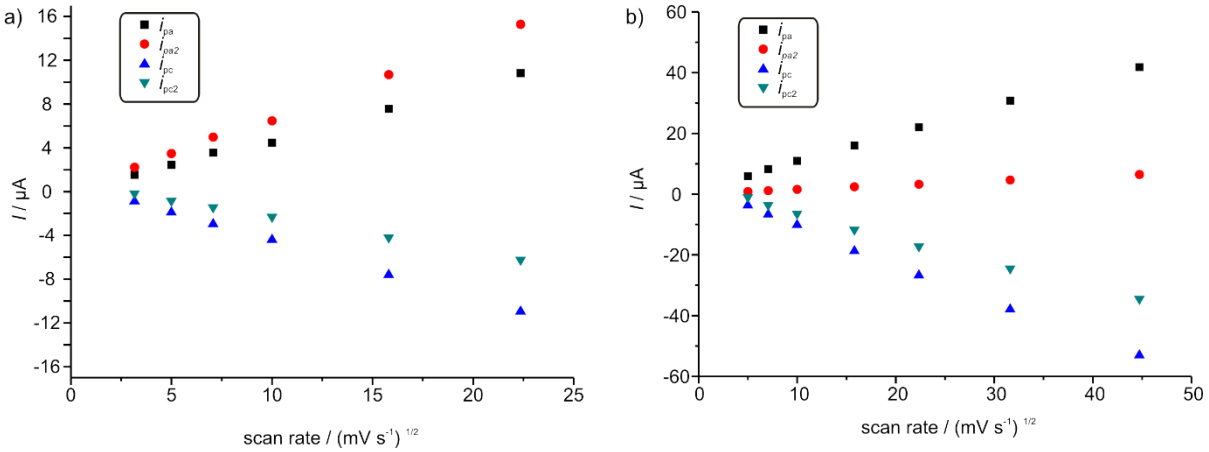

Fig. S13 Peak currents plotted against the square root of scan speed based on cyclic voltammograms of a) (*rac*)-**2** and b) (*rac*)-**2Ac** (CH_2Cl_2, with n-Bu_4NPF_6 as the electrolyte, 298 K). The peak currents can be approximated by linear functions, showing the reversibility of the redox process.

6. CD spectra

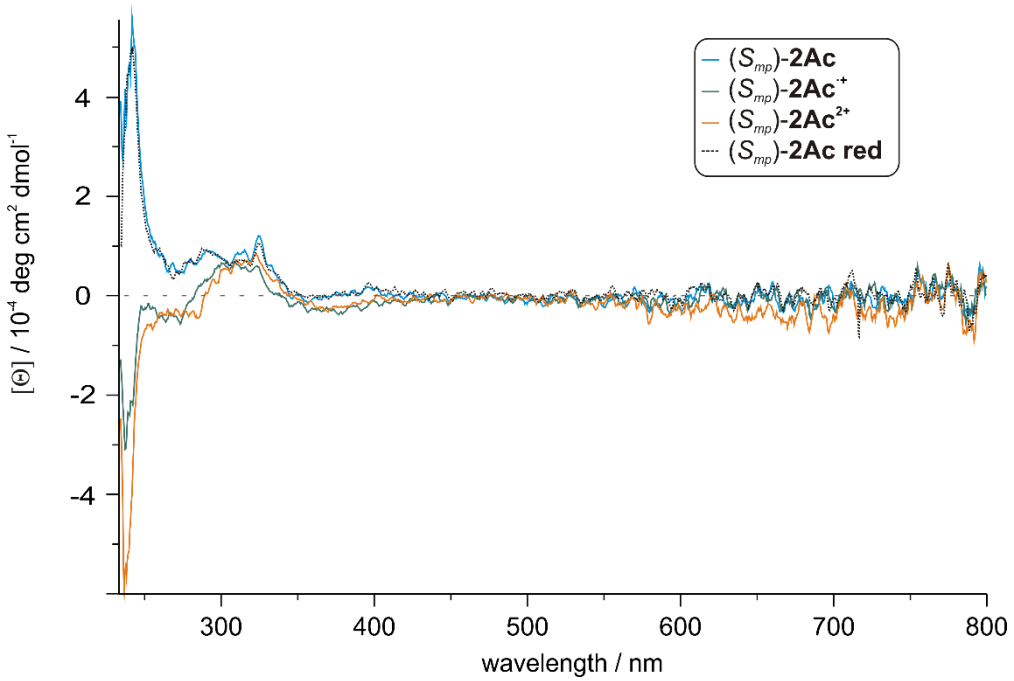

Fig. S14 CD spectra of (S_{mp})-**2Ac** (160 µM in CH_2Cl_2, 298 K, bulk $Fe(ClO_4)_3$ as the oxidant) in the TTF^0, $TTF^{\bullet+}$ and TTF^{2+} state and after reduction to the neutral form with Zn dust.

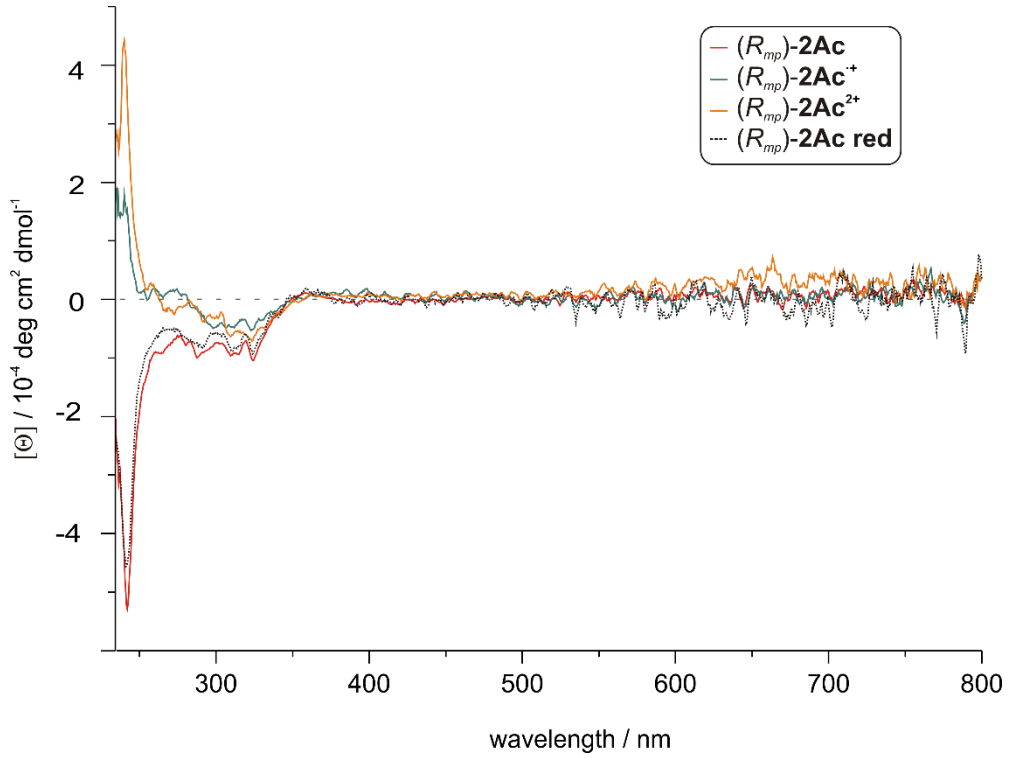

Fig. S15 CD spectra of (R_{mp})-**2Ac** (160 µM in CH_2Cl_2, 298 K, bulk $Fe(ClO_4)_3$ as oxidant) in the TTF^0, $TTF^{\bullet+}$ and TTF^{2+} state and after reduction to the neutral form with Zn dust.

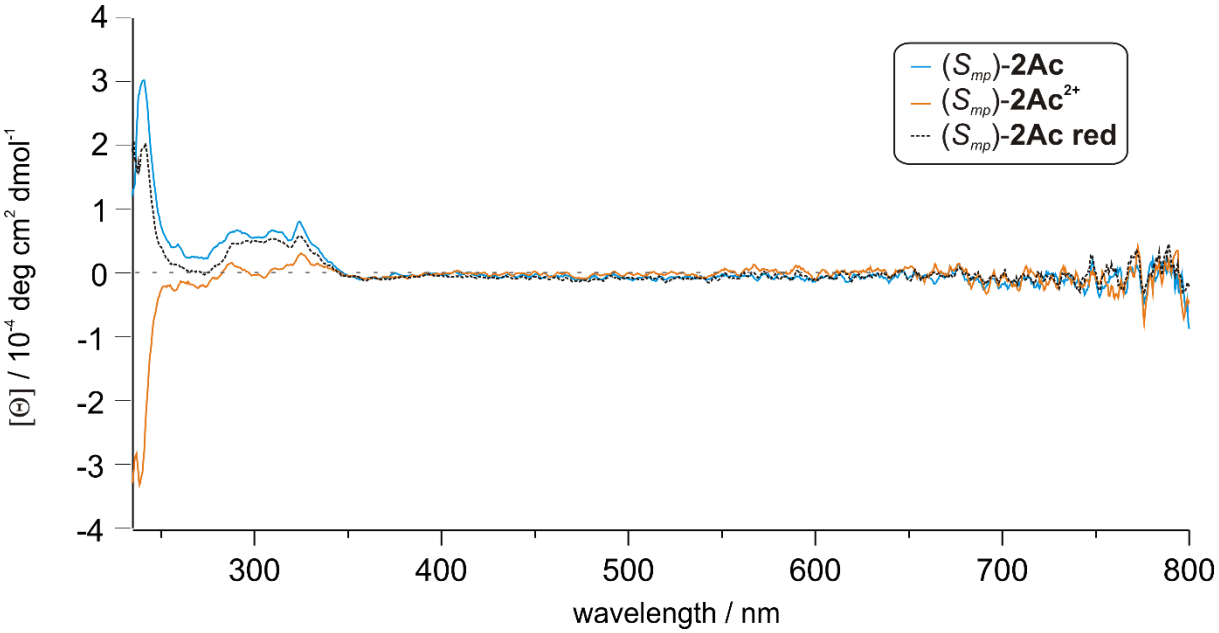

Fig. S16 CD spectra of (S_{mp})-**2Ac** (220 µM in ACN, 298 K, bulk $Fe(ClO_4)_3$ as the oxidant) in the TTF^0 and TTF^{2+} state and after reduction to the neutral form with Zn dust.

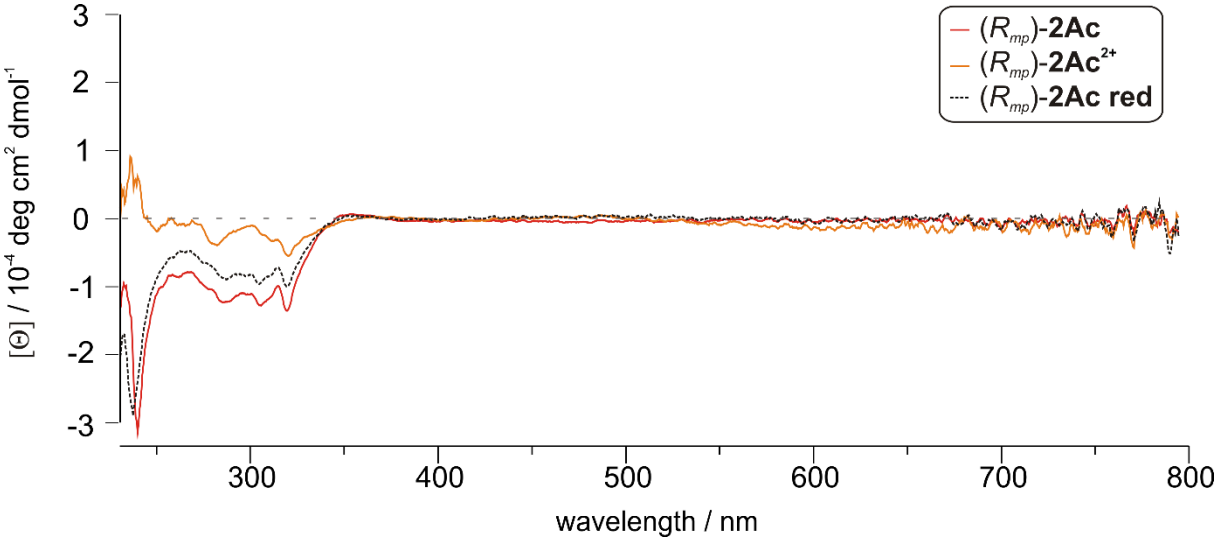

Fig. S17 CD spectra of (R_{mp})-**2Ac** (220 µM in ACN, 298 K, bulk $Fe(ClO_4)_3$ as oxidant) in the TTF^0 and TTF^{2+} state and after reduction to the neutral form with Zn dust.

7. Computational details

Conformational search. To study the influence of different conformations on the optical activity of *(*R_{mp}*)*-**2Ac**, we performed simulated annealing with the xTB (extended tight-binding) programme by Stefan Grimme.[13] This approach is based on DFTB (density functional tight binding)[14] and has been optimised for non-covalent interactions. GBSA (generalised Born accessible surface area)[15] was included as an implicit solvent model in the calculation. Using the Berendsen thermostat,[16] a maximum and minimum temperature of 1000 K and 300 K were chosen for annealing, respectively. The run time for each annealing step was 50 ps, the time step was 2 fs, and structures were dumped every 50 fs. Furthermore, the SHAKE algorithm[17] was applied to restrain hydrogen atoms from dissociating.

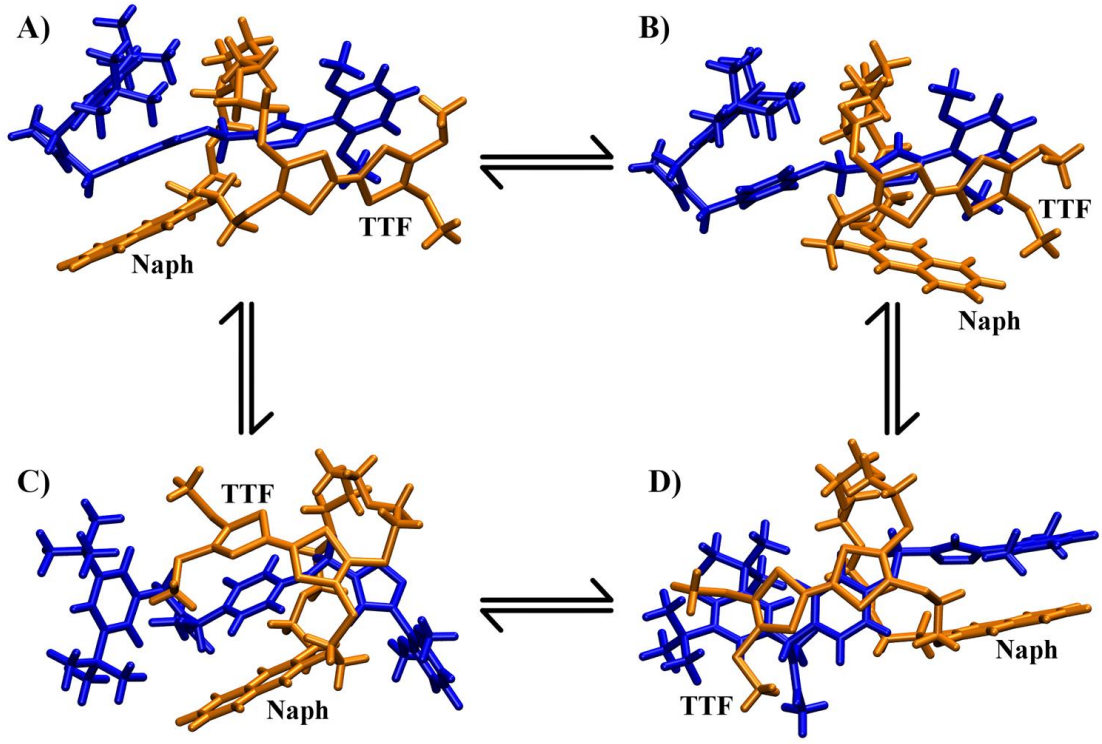

Fig. S18: The four most favourable conformations of (*R_{mp}*)-**2Ac**: **A**, **B**, **C**, and **D**. The conformations differ in the way the TTF core, the naphthalene unit, and the axle are positioned with respect to each other. Every conformation can be interconverted into another by flipping the TTF or the naphthalene unit or both.

Fig. S18 displays the four most stable conformations re-optimised at the RI*J*-TPSS-D3(BJ)/def2-SVP[18-22] level of density functional theory (DFT) with the programme package Turbomole (version 7.1)[23]. COSMO (ε = 8.9 for CH_2Cl_2)[24] was employed as the solvent model. Subsequent single-point calculations to assess the relative stabilities of the four conformations (see Table S2) were performed at the RI*J*COSX-ωB97X-D3/def2-TZVP[25, 26] level with CPCM[27]

as solvent model using ORCA (version 4.0.1)[28]. Finally, Grimme's sTD-DFT (simplified time-dependent DFT)[29] approach was used at the same level to connect electronic properties and optical activity, i.e. the ECD spectra (Fig. 4 in main text) of (R_{mp})-**2Ac**. The entire procedure was conducted for both (R_{mp})-**2Ac** and (R_{mp})-**2Ac^{2+}**.

Tab. S2: Relative electronic energies of all conformations in charge states 0 and 2+ calculated at the ωB97X-D3 level of DFT (values in kJ/mol)

charge state	conformer A	conformer B	conformer C	conformer D
0	0.0	30.4	43.9	17.9
2+	8.5	0.0	54.6	58.6

Calculations at other levels of theory (PBE0[30], CAM-B3LYP[31], and M06-2X[32]) confirm the relative stabilities of the four conformers. Moreover, the shapes of the simulated ECD spectra are considered reliable as they agree with each other regarding the signs of the CD bands. Nevertheless, a systematic red-shift in wavelengths of sometimes up to 50 nm compared to experiment is observed, which is however expected for different density functionals (see Fig. S19 for an illustrative example).

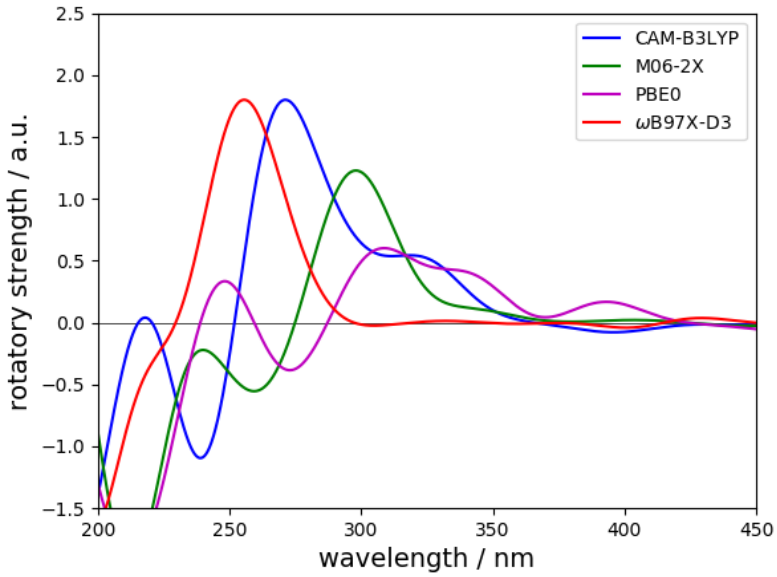

Fig. S19: ECD spectra of (R_{mp})-**2Ac**$^{2+}$ in conformation **A** computed at the sTD-DFT level with various functionals. Gaussian line broadening with σ = 20 nm was applied. Vertical transition lines are omitted for clarity. It can be observed that the general shapes of the spectra agree while the absolute positions of the signals vary in wavelengths to some extent.

Furthermore, it should be noted that (R_{mp})-**2Ac**$^{2+}$ in all four conformations displays non-negligible rotarory strengths for the TTF-centered transition at around 650-700 nm (not shown in Fig. S19) which is caused by an overestimation of the magnetic dipole transition moment

owing to a seemingly poor description of the TTF-TTF transition within the sTD-DFT framework.

Electronic structure and transitions.

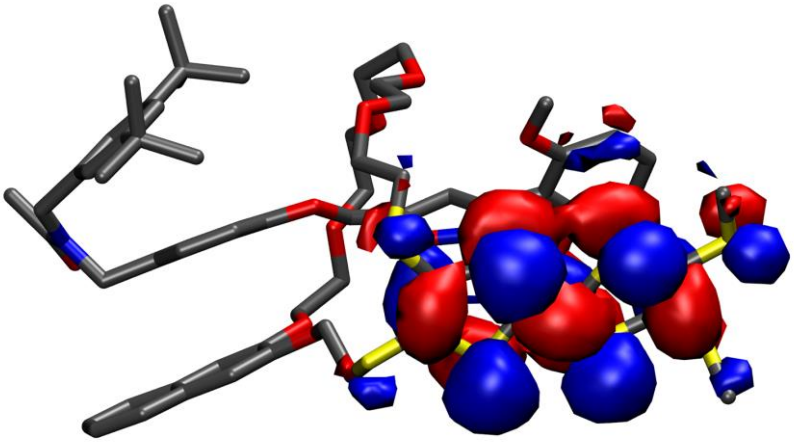

Fig. S20: HOMO of **2Ac** in conformation **A** (the same nodal shape can be observed for the LUMO of **2Ac**$^{2+}$), isovalue = 0.01 a_0^{-3}.

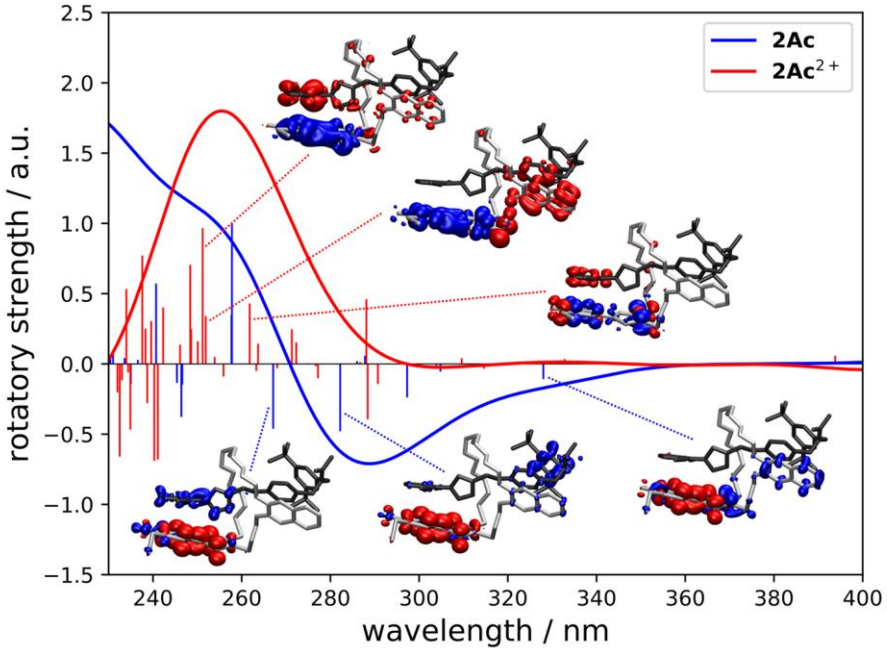

Fig. S21: Simulated ECD spectra of (R_{mp})-**2Ac** and (R_{mp})-**2Ac^{2+}** both in conformation **A** obtained at the ωB97X-D3/def2-TZVP level of sTD-DFT. Gaussian line broadening with σ = 20 nm was applied. Insets: Excited state difference densities of selected transitions to visualise the electron flow during these excitations. Blue and red zones correspond to areas of electron-enhancement and electron-depletion, respectively. Isovalue: 0.001 a_0^{-3}.

Intramolecular interactions. An atoms-in-molecules (AIM)[33] bonding analysis was performed for *(R_{mp})*-**2Ac** in all *four* conformations and charge state 0 and 2+. Fig. S22 shows *(R_{mp})*-**2Ac** in conformation **A** with its bond critical points as a representative example. An AIM analysis is useful for studying non-covalent interactions. C-H···π and π-π-stacking interactions can thus be easily identified within *(R_{mp})*-**2Ac**. Together with the results from our DFT calculations at the RI*J*COSX-ωB97X-D3/def2-TZVP level, we can deduce what is likely responsible for the conformational behaviour of *(R_{mp})*-**2Ac** and *(R_{mp})*-**2Ac**$^{2+}$. Important aspects are the energetic gain through π-π-stacking between the various (aromatic) units and the delocalisation of electron density near the TTF unit.

First, we will discuss the neutral molecule *(R_{mp})*-**2Ac**. Conformation **A** exhibits a large amount of intramolecular interactions especially through π-π-stacking of aromatic units. Furthermore, the TTF unit's proximity to the isoxazole core and the dimethoxy-phenyl moiety yield non-covalent interactions. In conformation **B**, many of the π-π-stacking interactions are lost as the naphthalene moiety attaches itself to the TTF unit, which makes this conformation around 30 kJ/mol less stable. The energetic gain in conformation **D** is based on the interaction

between the naphthalene, the isoxazole core, and the dimethoxy-phenyl unit and the stacking of the TTF unit and the phenyl spacer. However, the di-*tert*butyl-phenyl unit is not able to stack with any of the other aromatic units anymore, which results in a net loss of almost 18 kJ/mol with respect to conformation **A**. Finally, conformation **C** is the least stable structure (ca. 44 kJ/mol with respect to **A**) since effective π-π-stacking is neither achieved by the isoxazole unit nor by the dimethoxy-phenyl ring nor by the di-*tert*butyl-phenyl moiety. The energetic gain through non-covalent interactions is solely based on the arguably inefficient stacking between TTF core, phenyl spacer and naphthalene unit.

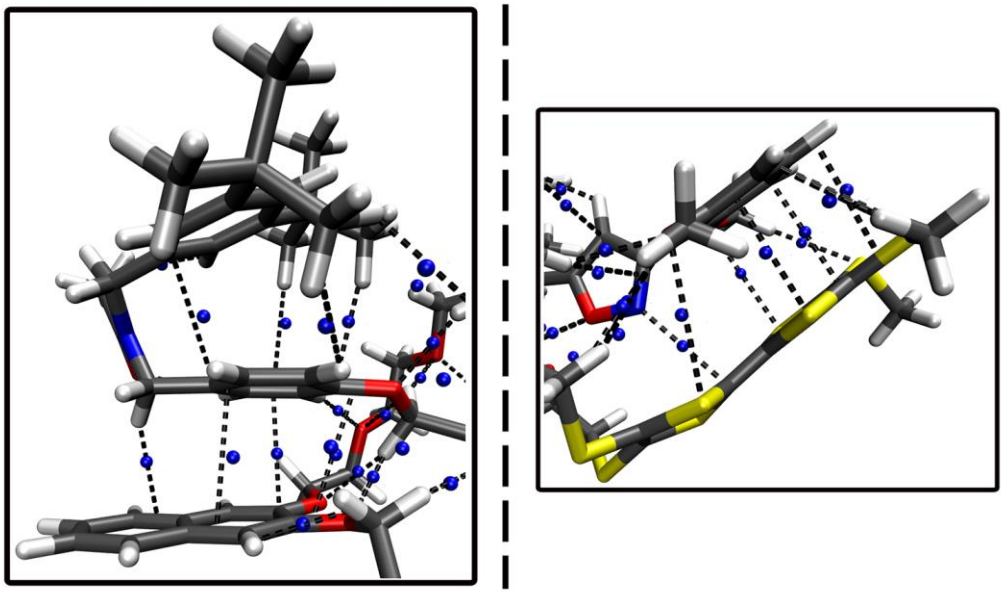

Fig. S22: Bond critical points (blue spheres) obtained at the ωB97X-D3/def2-TZVP level utilising the Multiwfn programme[34] near the naphthalene moiety (left) and the TTF unit (right) illustrating the non-covalent interactions within **2Ac** in conformation **A**.

For *(R_{mp})*-**2Ac**$^{2+}$ the picture is quite different. Now conformation **B** is the most stable structure since the charge, which is mostly localised on the TTF unit, can be delocalised over the TTF core, the naphthalene unit, the isoxazole ring, and the dimethoxy-phenyl moiety. Additionally, there is still the π-π-stacking interaction between the di-*tert*butyl-phenyl unit and the phenyl spacer contributing to its energetic stability. The charge delocalisation over four different units in the molecule is missing in conformation **A**, which makes it somewhat less stable than **B** (~ 9 kJ/mol). Similar arguments account for conformation **D**, which is – maybe somewhat surprisingly - by far the least stable structure now (over 58 kJ/mol), as the charge is not efficiently delocalised which seems to massively overcompensate any π-π-stacking interactions. In conformation **C**, the charge can be somewhat better delocalised than in **D**,

however, due to its lack of more efficient π-π-stacking interactions it is also somewhat less stable than **B** (ca. 55 kJ/mol).

8. Crystallographic data

General details. Single crystal X-ray data in the present study were collected at 170 K on a Bruker-Nonius KappaCCD diffractometer with APEX-II detector and graphite monochromatized Mo-Kα (λ = 0.71073 Å) radiation. The *COLLECT*[35] software was used for data collection (θ and ω scans) and *DENZO-SMN*[36] for the processing. Lorentzian polarization correction was applied on all data and absorption effects were corrected with multi-scan method (*SADABS*[37]). The structures were solved by intrinsic phasing methods (*SHELXT*[38]) and refined by full-matrix least squares on F^2 using *SHELXL*-2018/3.[39] The *SQUEEZE* module of *PLATON*[40, 41] was utilized in the structure refinement to remove the residual electron densities, which could not be reliably assigned and refined. Anisotropic displacement parameters were assigned to non-H atoms. Positional disorder in the structures was treated by gently restraining geometric and anisotropic displacement parameters. All hydrogen atoms were refined using riding models with U_{eq}(H) of 1.5U_{eq}(C) for terminal methyl groups and of 1.2U_{eq}(C) for other groups. The main details of crystal data collection and refinement parameters are presented below. CCDC 1910670 contains the supplementary crystallographic data for this paper. These data can be obtained free of charge via http://www.ccdc.cam.ac.uk/conts/retrieving.html (or from the CCDC, 12 Union Road, Cambridge CB2 1EZ, UK; Fax: +44 1223 336033; E-mail: deposit@ccdc.cam.ac.uk).

Structure of dTTFC8: Compound **dTTFC8** was crystallised as orange needles with vapour diffusion of Et_2O into CH_2Cl_2 solution of the compound. Crystal data and refinement parameters of **dTTFC8**: $C_{30}H_{36}O_6S_8$, M = 749.07, monoclinic, space group $P2_1/n$ (no. 14), a = 25.1361(6), b = 5.09490(10), c = 30.6018(9) Å, β = 109.649(2)°, V = 3690.8(2) Å^3, Z = 4, ρ_{calc} = 1.348 Mgm^{-3}, μ = 0.522 mm^{-1}, F_{000} = 1568, θ range = 1.82-26.37°, 14025 reflections collected of which 7554 unique (R_{int} = 0.1129), No. of reflections with $I>2\sigma(I)$ = 3856, which were used in all calculations, 409 parameters and 32 restraints, Goodness-of-fit (F^2) = 1.018. The final R indices [$I>2\sigma(I)$]: R1 = 0.0734 and wR2 = 0.1436. R indices (all data): R1 = 0.1606 and wR2 = 0.1770. Largest residual electron densities: 0.598 and -0.408 e.Å^{-3}.

Structure description for dTTFC8: Crystal structure solution of **dTTFC8** shows nicely that the substituted TTF is attached to the naphthalene crown ether macrocycle. There is a slight disorder in one oxygen atom of crown ether, which is divided over two spatial positions. The substituted TTF moiety exhibits typical bond distances for neutral TTF derivatives,[42-44] like

characteristically short C=C distance of 1.345(7) Å between the 1,3-dithiole rings and a distance range of 1.749(6) to 1.764(5) Å for C-S bonds. An Interesting geometric feature is the planarity of substituted TTF moiety with both 1,3-dithiole rings and all S atoms, as well lying in the same plane. The notably acute angle between the naphthalene and TTF planes (74.8°) can be attributed to the connecting ethylene bridge which avoids ecliptic and gauche conformations by maintaining an OCCS dihedral angle of 159.4°. In the crystal packing, the molecules are arranged in columnar stacks. Naphthalenes stack with naphthalenes with a plane-to-plane distance of 3.29 Å shifted sideways by 3.88 Å and TTFs on top of each other. Instead, TTFs stack with plane-to-plane distances of 3.47 Å, and a sideways slip of 3.73 Å, respectively.

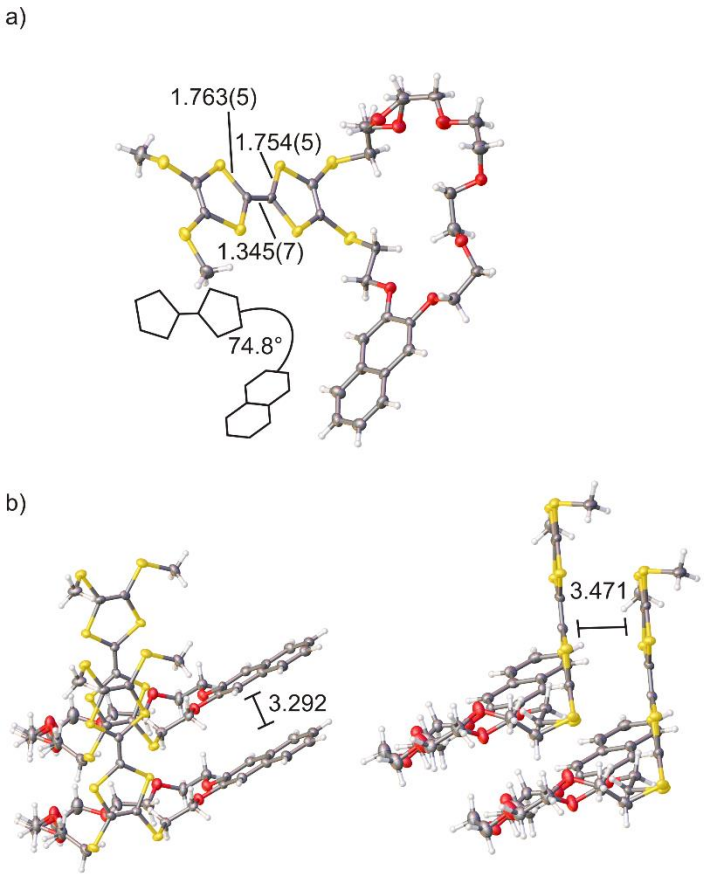

Figure S23: Solid-state structure of **dTTFC8**. (a) Top view with selected bond lengths (Å) and the angle between the naphthalene and the TTF plane. (b) Side view of two stacked **dTTFC8** molecules in the crystal with distances (Å) between molecule planes. Colour codes: S = yellow; O = red; C = grey; H = black (spheres).

9. ^{1}H, ^{13}C NMR

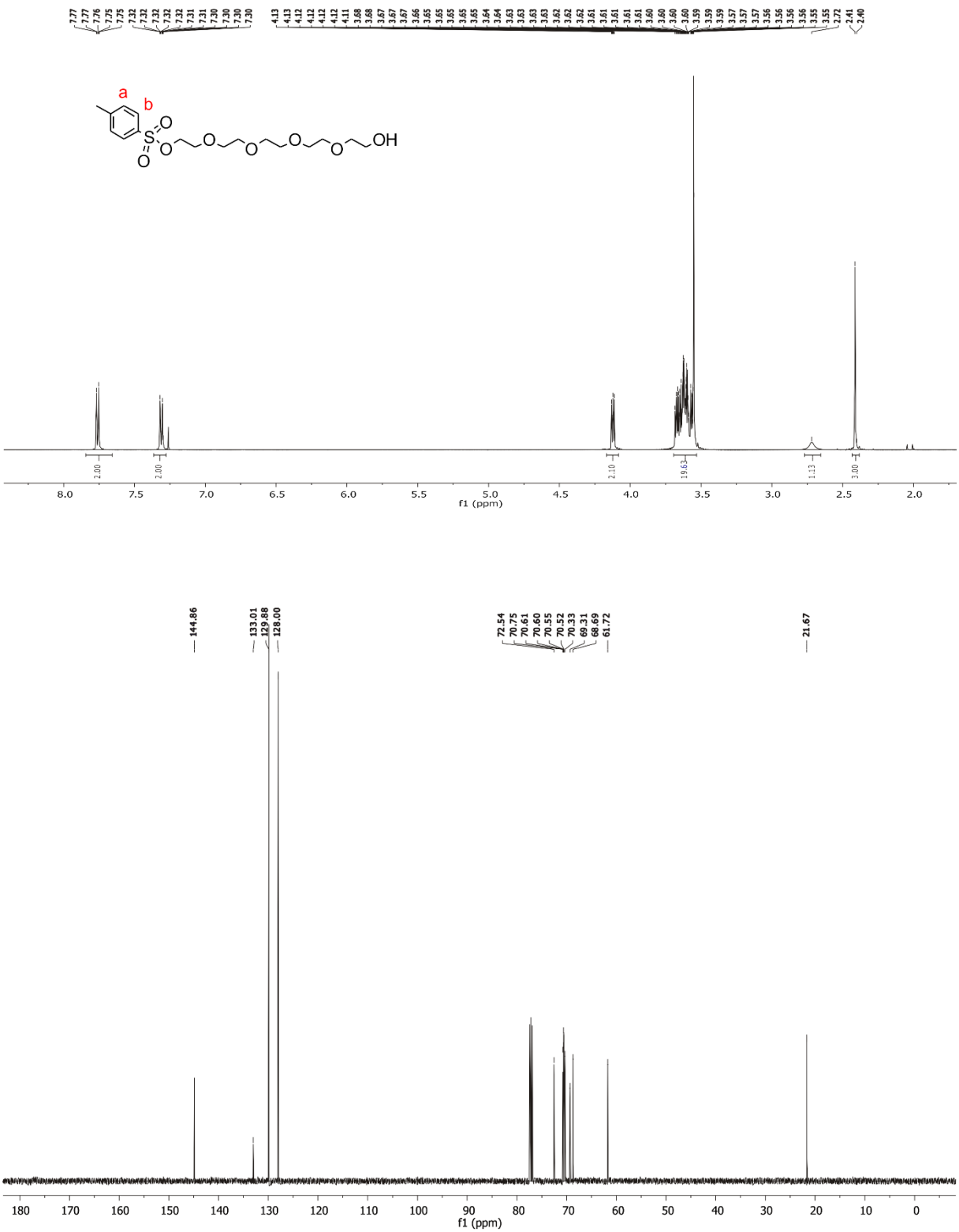

Fig. S24 ^{1}H (top) and ^{13}C (bottom) NMR spectrum (500/126 MHz, $CDCl_3$, 298 K) of **S2**.

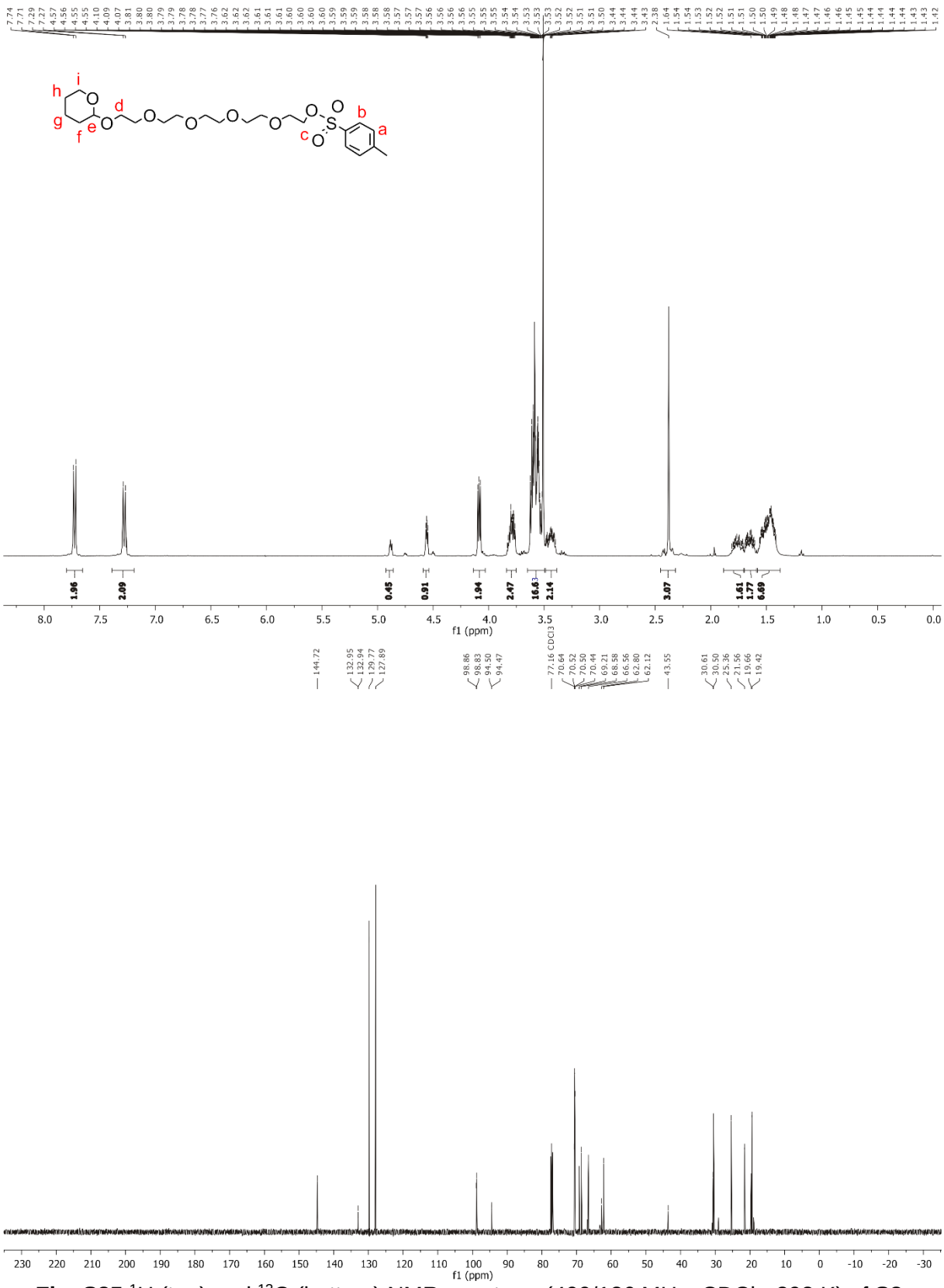

Fig. S25 ^{1}H (top) and ^{13}C (bottom) NMR spectrum (400/126 MHz, $CDCl_3$, 298 K) of **S3**.

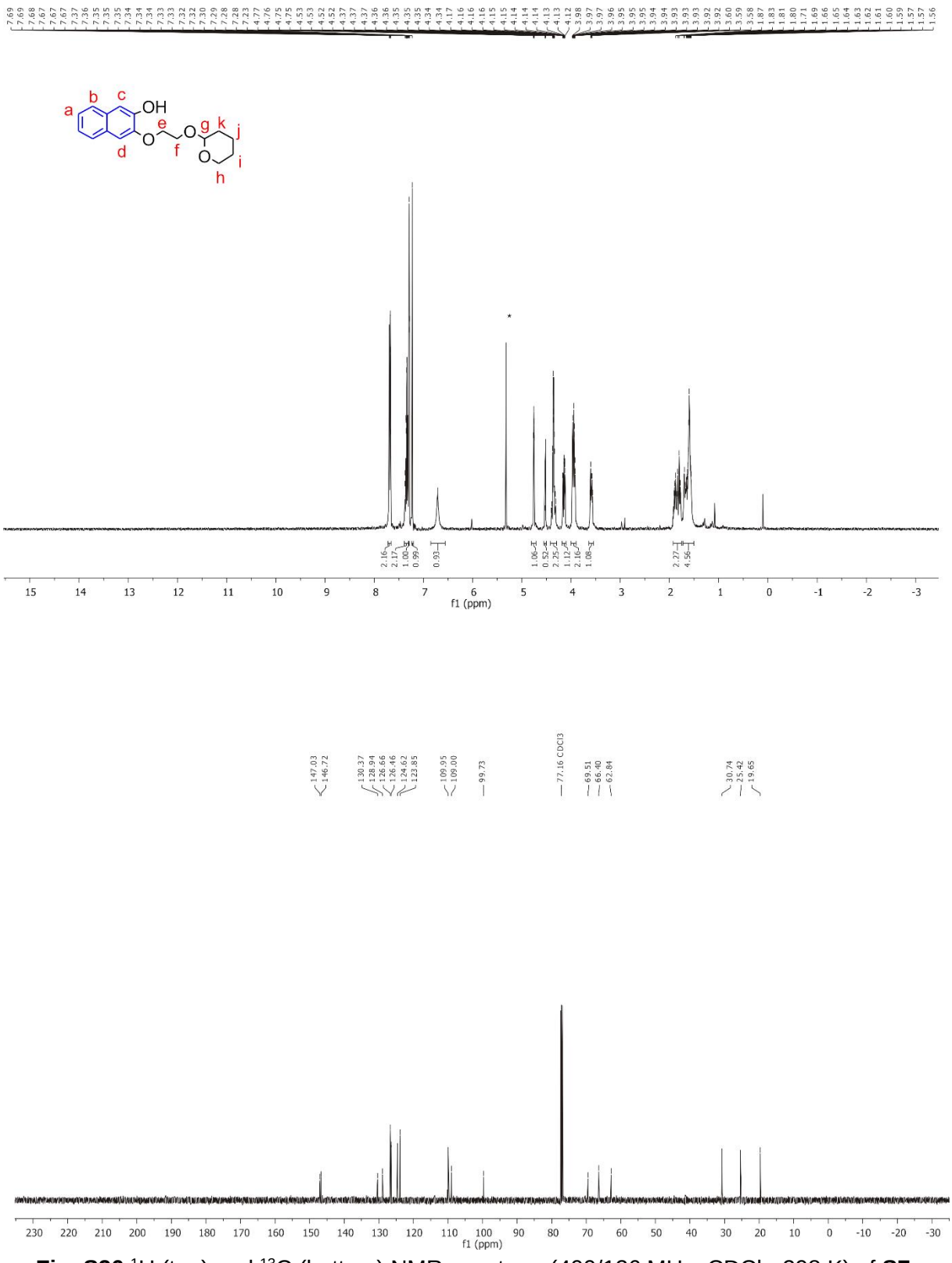

Fig. S26 ^{1}H (top) and ^{13}C (bottom) NMR spectrum (400/126 MHz, $CDCl_3$, 298 K) of **S7**.

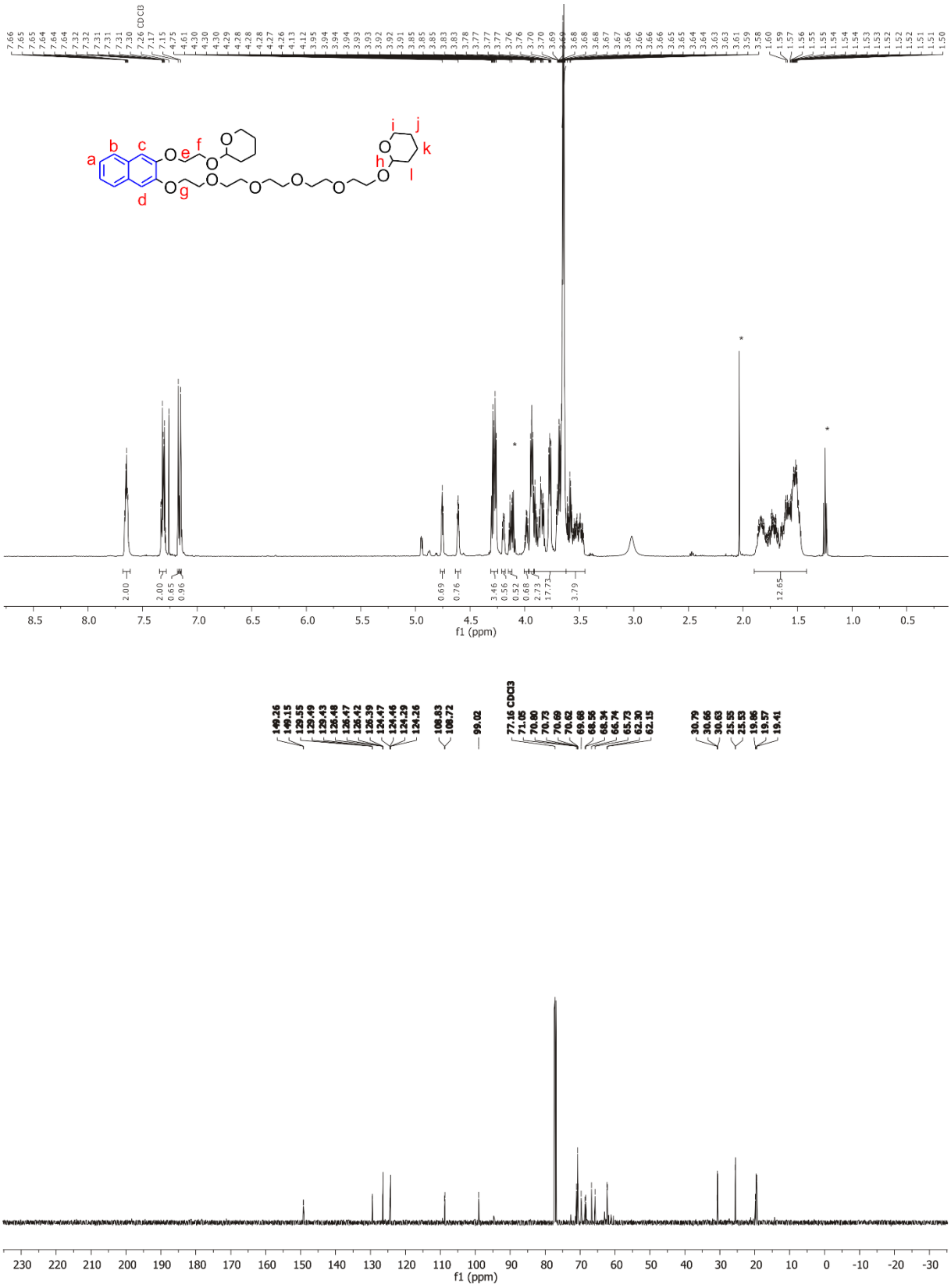

Fig. S27 ^{1}H (top) and ^{13}C (bottom) NMR spectrum (500/126 MHz, $CDCl_3$, 298 K) of **S8**.

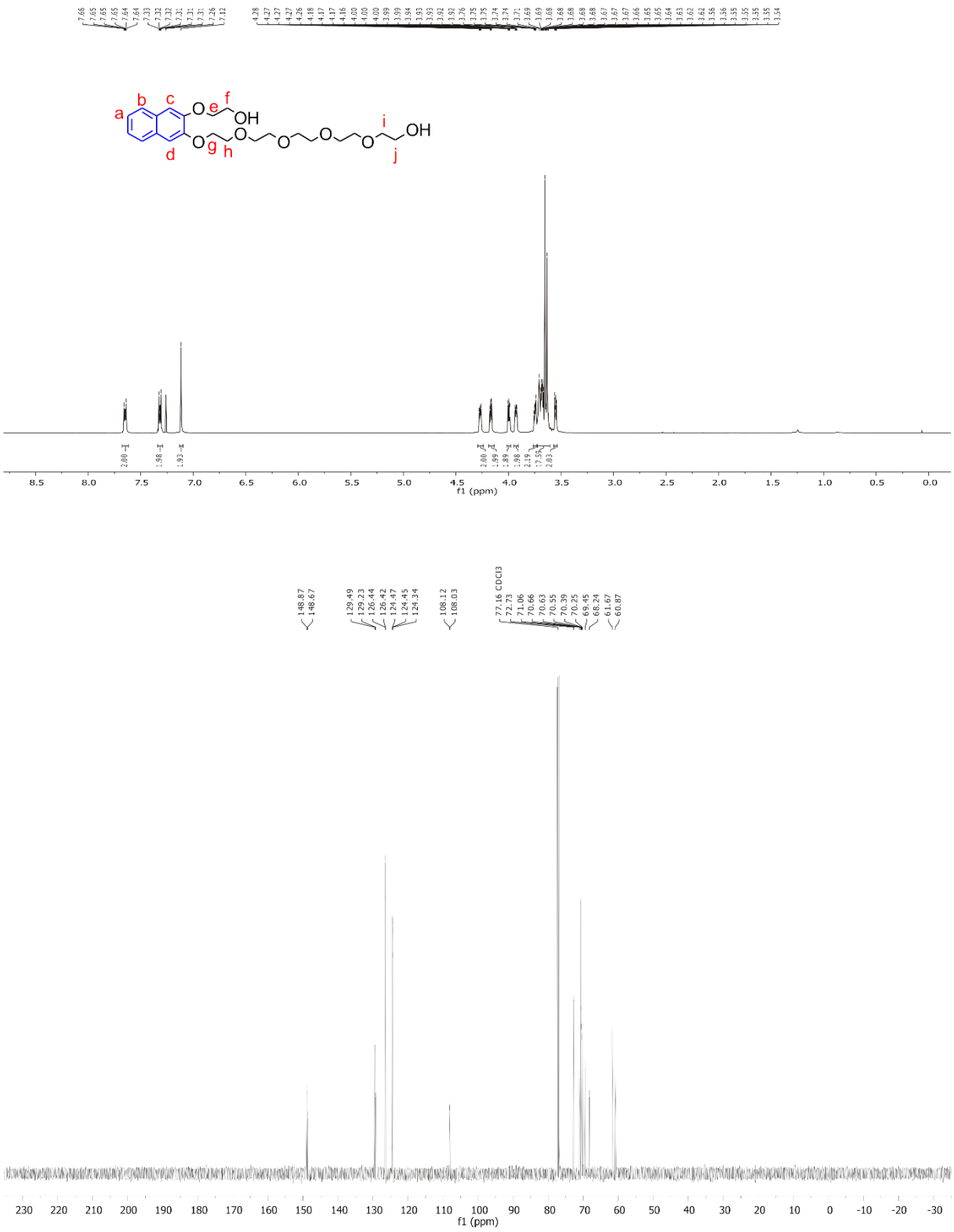

Fig. S28 ^{1}H (top) and ^{13}C (bottom) NMR spectrum (500/126 MHz, $CDCl_3$, 298 K) of **S9**.

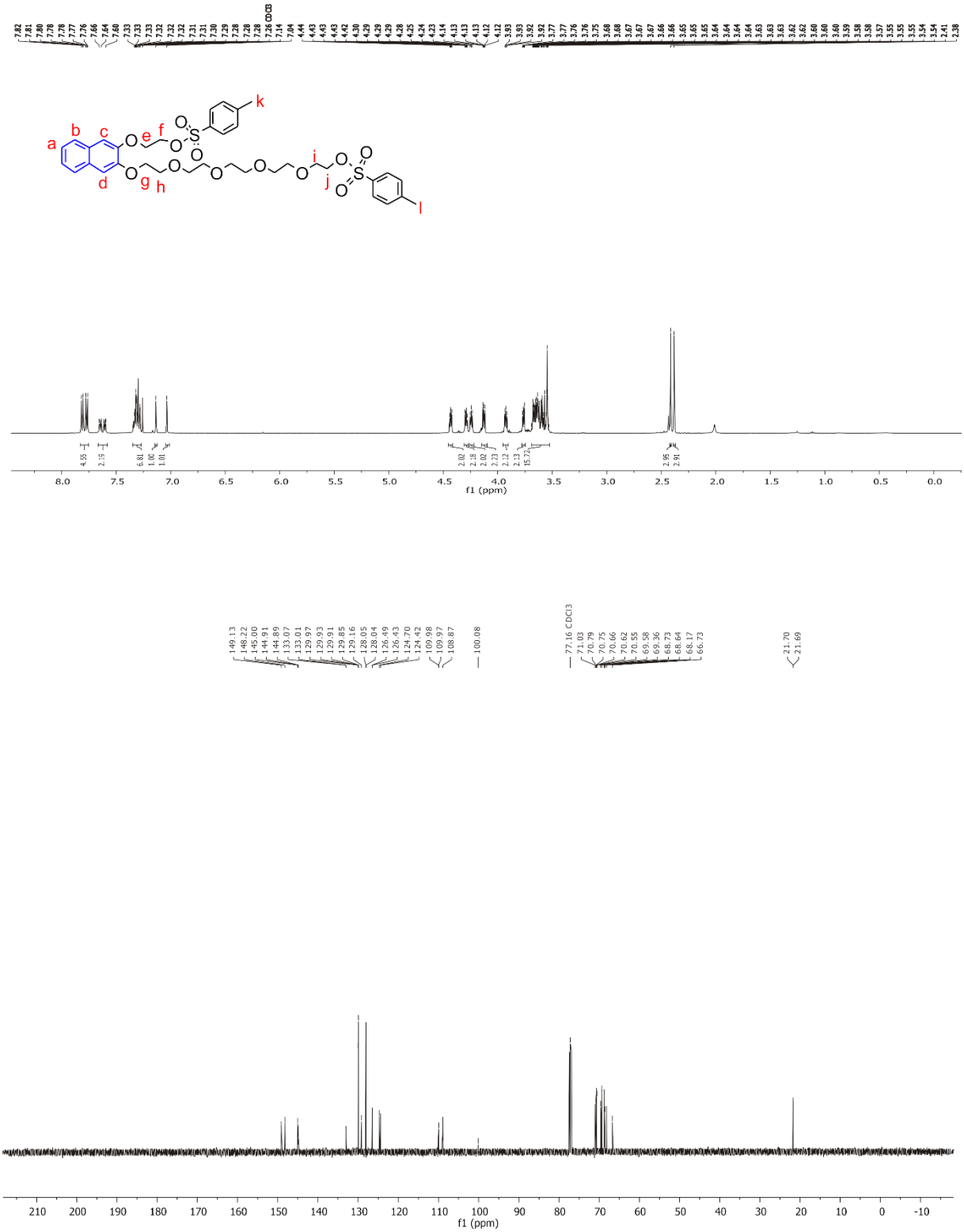

Fig. S29 ^{1}H (top) and ^{13}C (bottom) NMR spectrum (500/126 MHz, $CDCl_3$, 298 K) of **S10**.

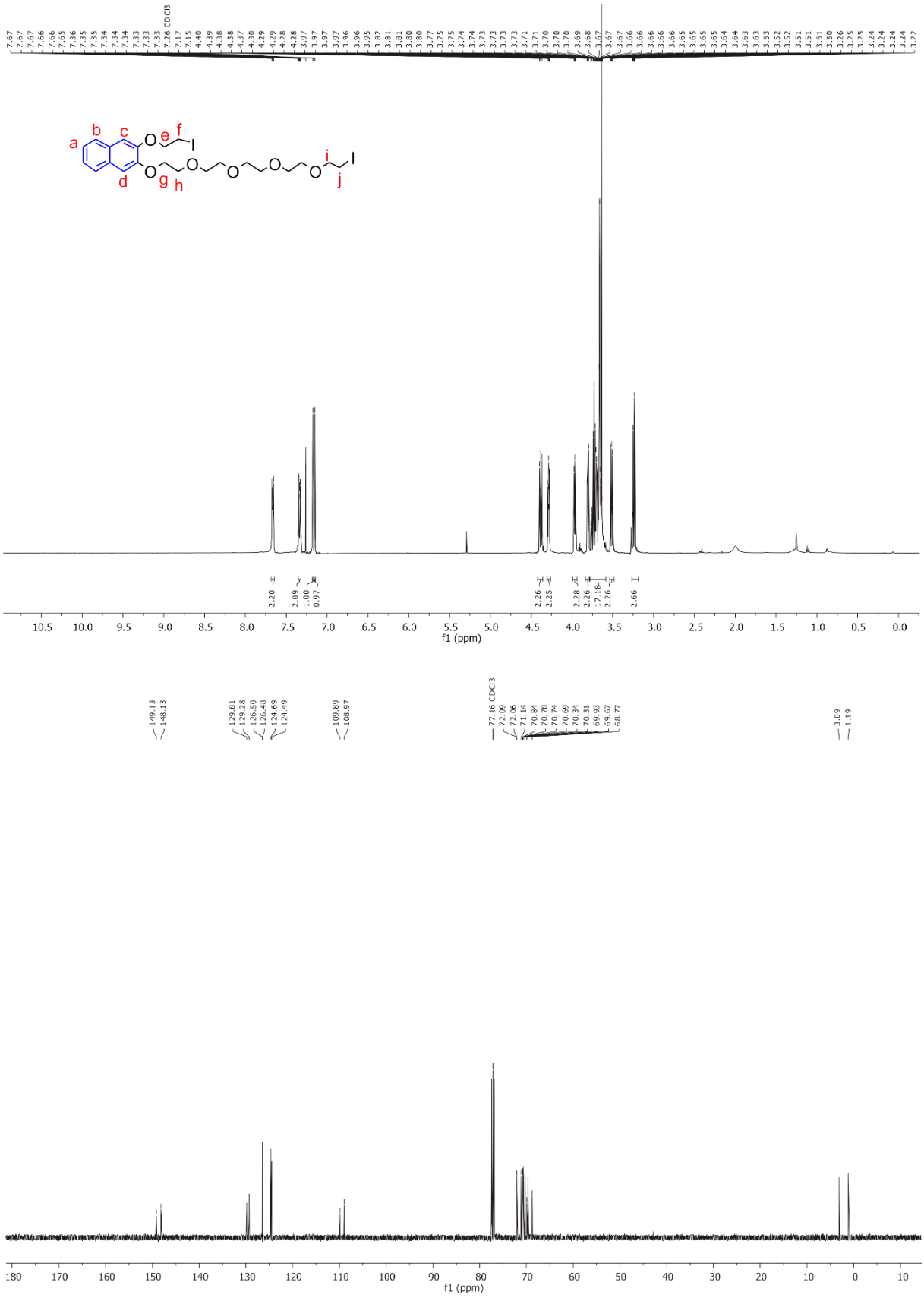

Fig. S30 ^{1}H (top) and ^{13}C (bottom) NMR spectrum (500/126 MHz, $CDCl_3$, 298 K) of **S11**.

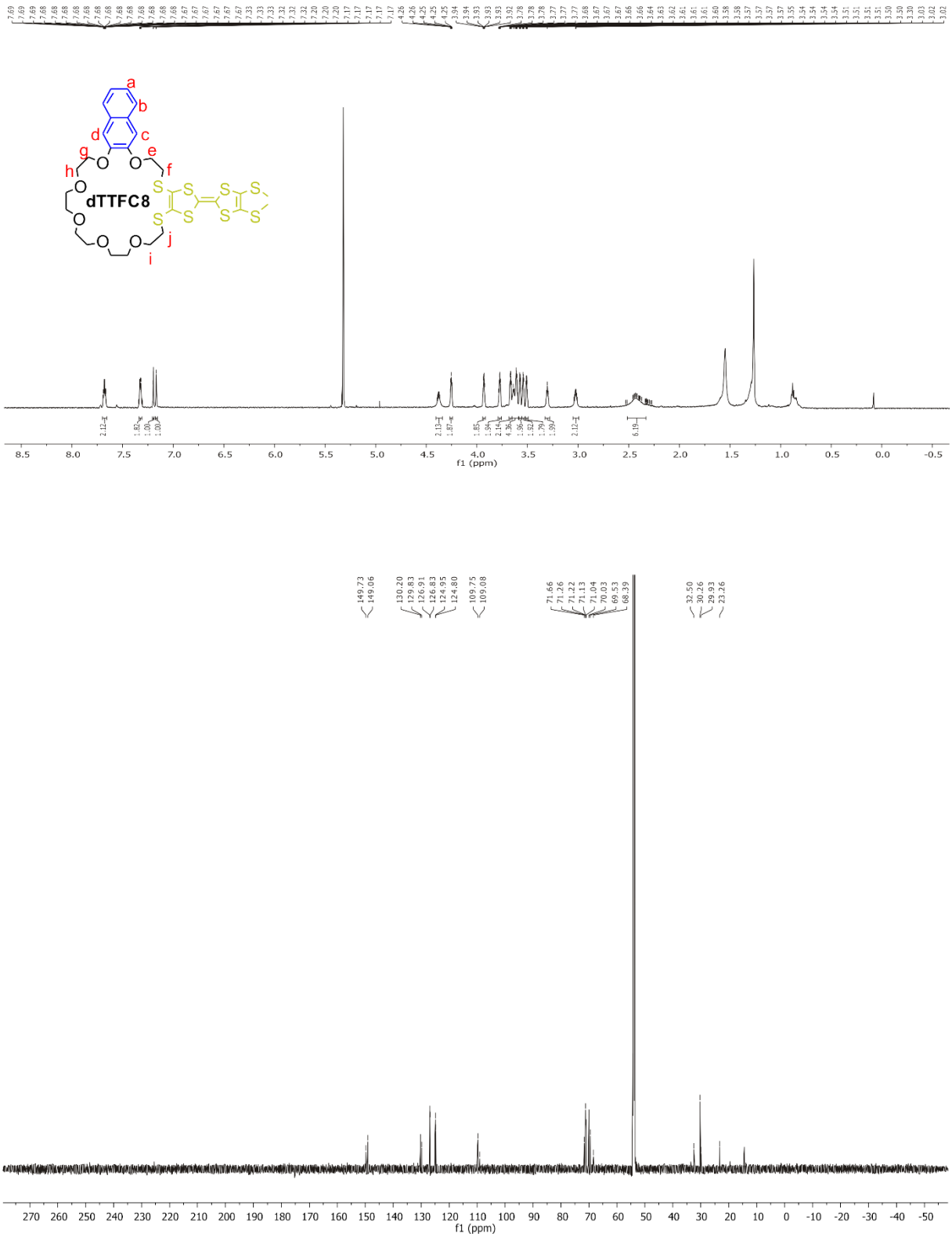

Fig. S31 ^{1}H (top) and ^{13}C (bottom) NMR spectrum (700/176 MHz, $CDCl_3$, 298 K) of **dTTFC8**.

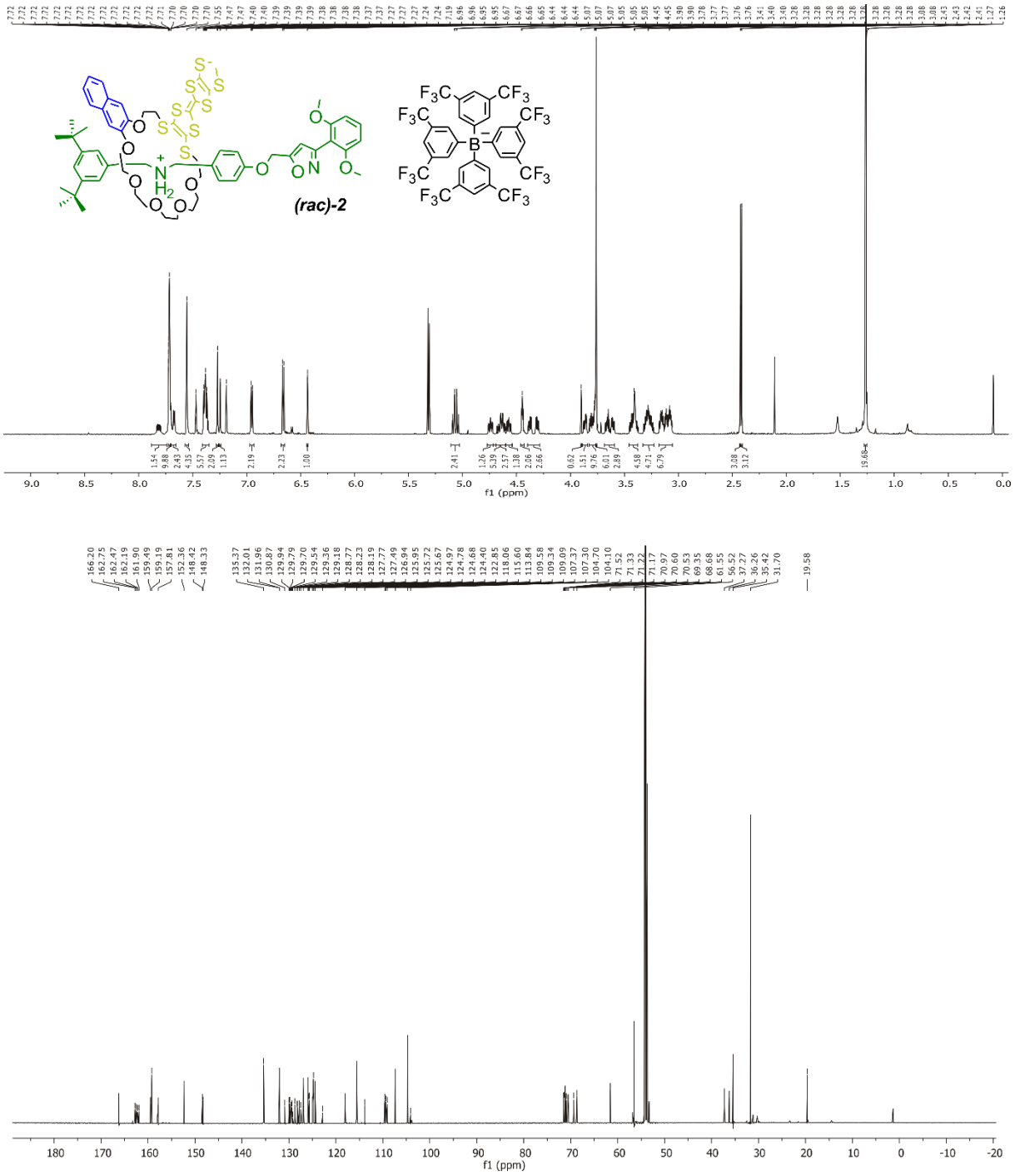

Fig. S32 ^{1}H (top) and ^{13}C (bottom) NMR spectrum (700/176 MHz, CD_2Cl_2, 298 K) of the racemic mixture of **2**.

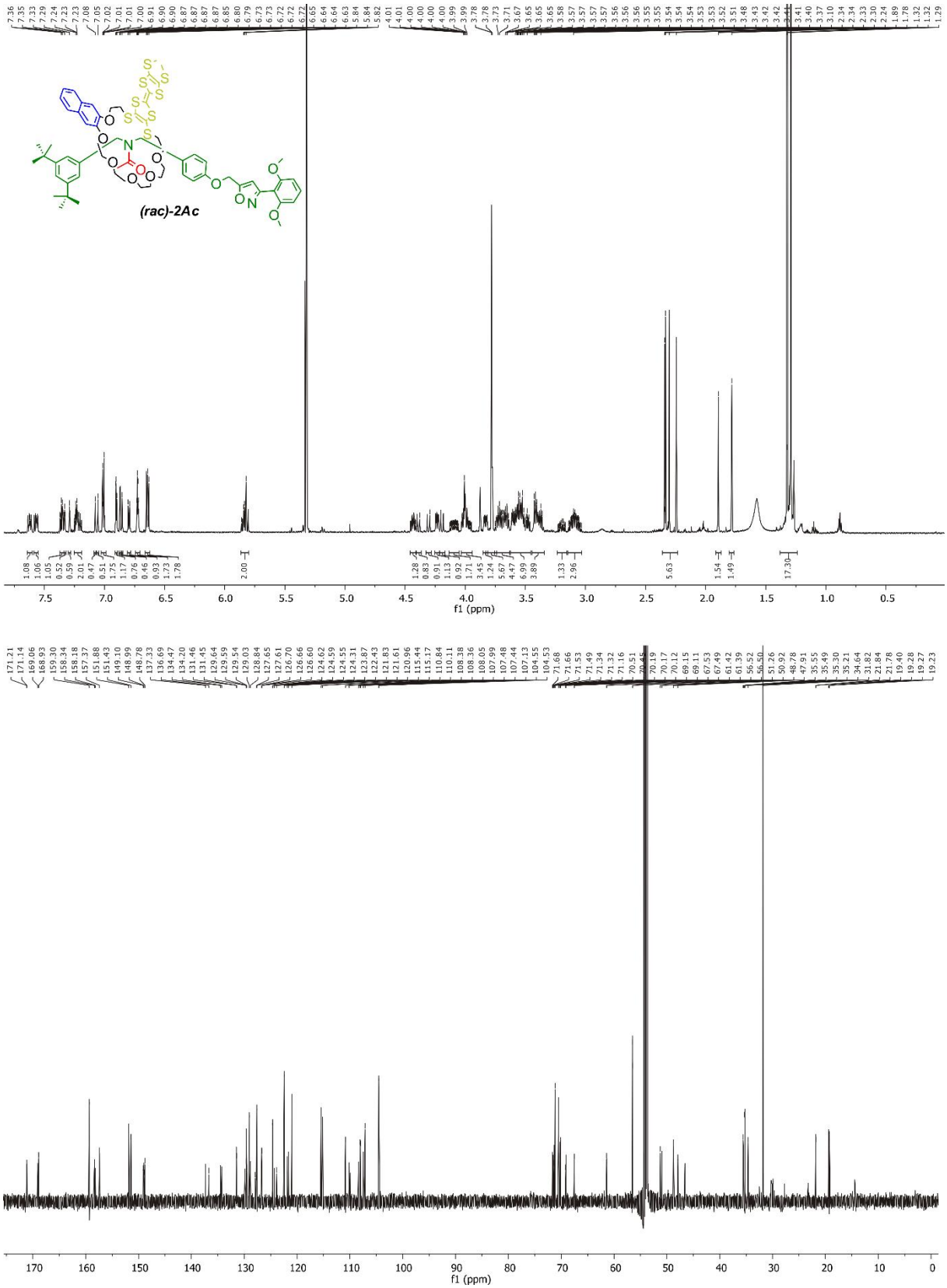

Fig. S33 ^{1}H (top) and ^{13}C (bottom) NMR spectrum (700/176 MHz, CD_2Cl_2, 298 K) of the racemic mixture of **2Ac**.

9. HR-MS

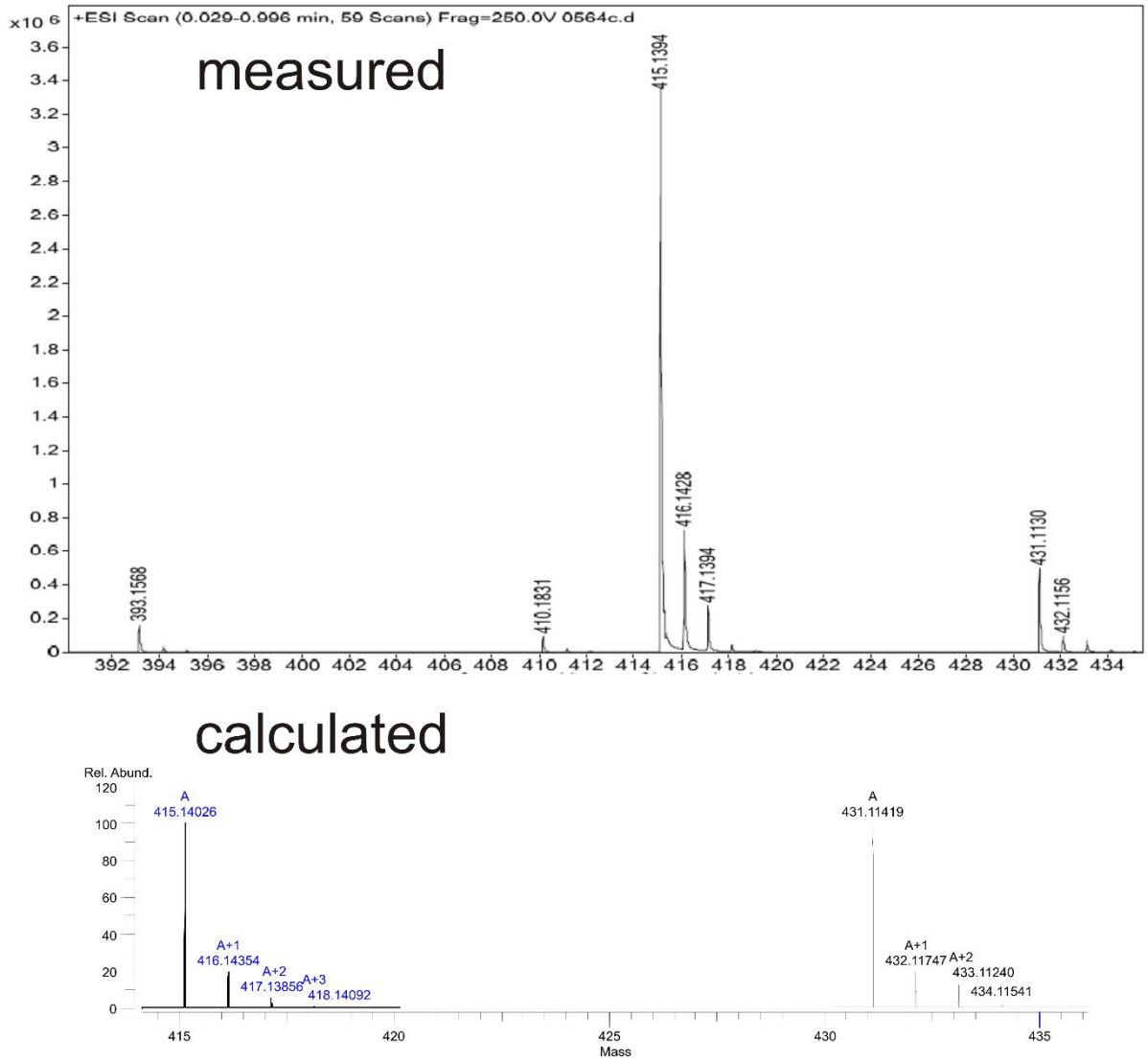

Fig. S34 HRMS ESI$^+$ (top) and calculated (bottom) of **S2**.

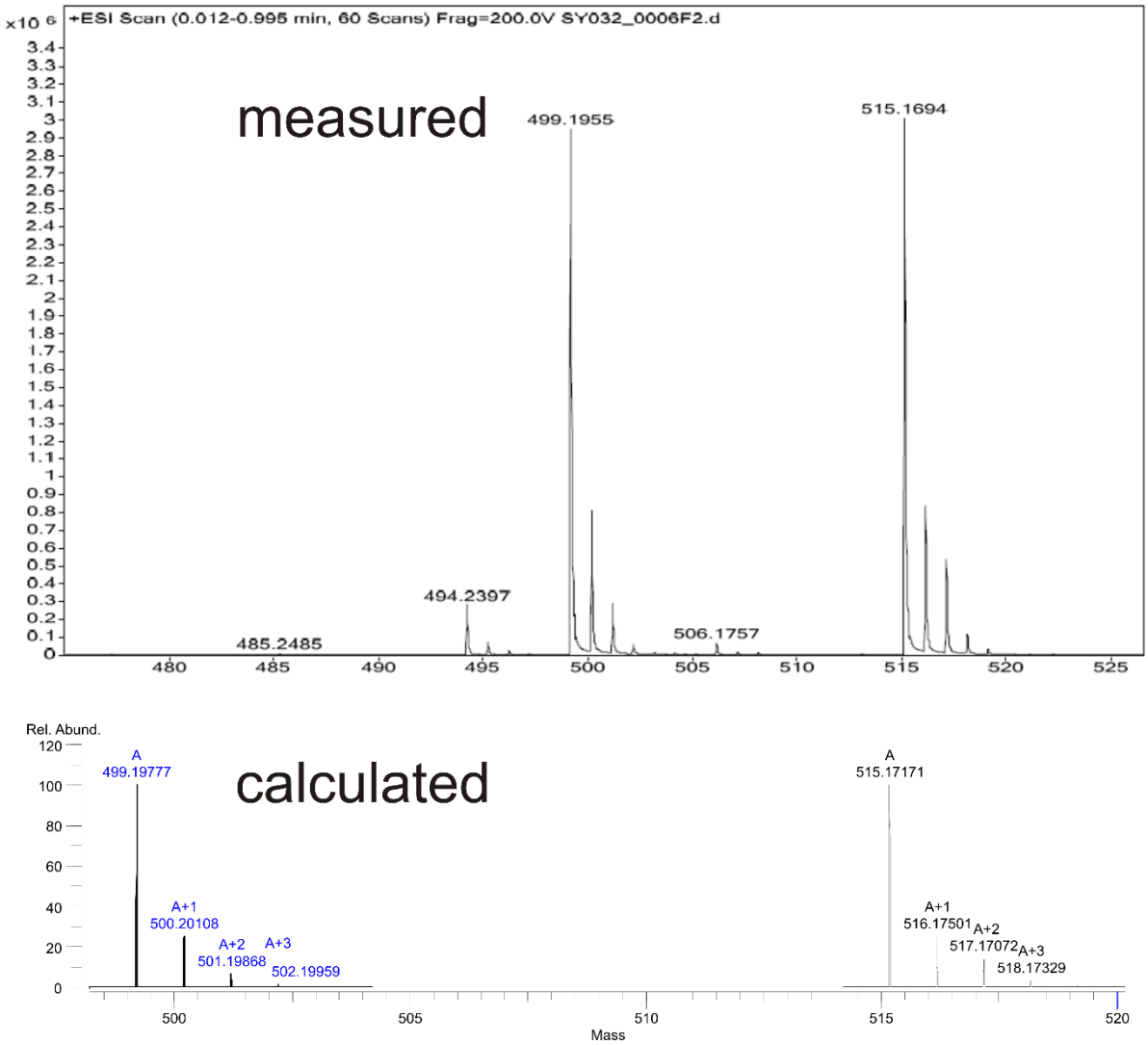

Fig. S35 HRMS ESI$^+$ (top) and calculated (bottom) of **S3**.

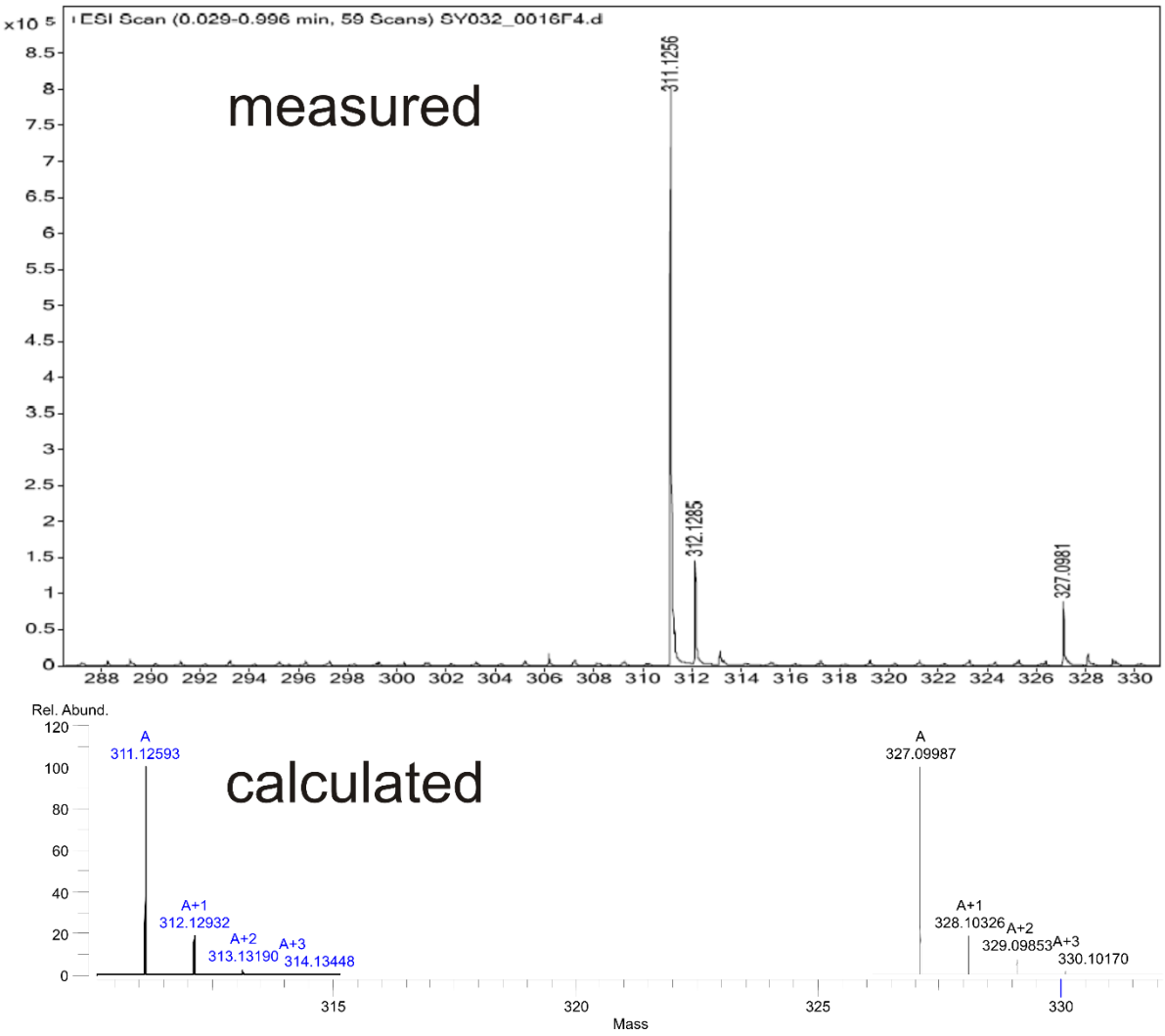

Fig. S36 HRMS ESI$^+$ (top) and calculated (bottom) of **S7**.

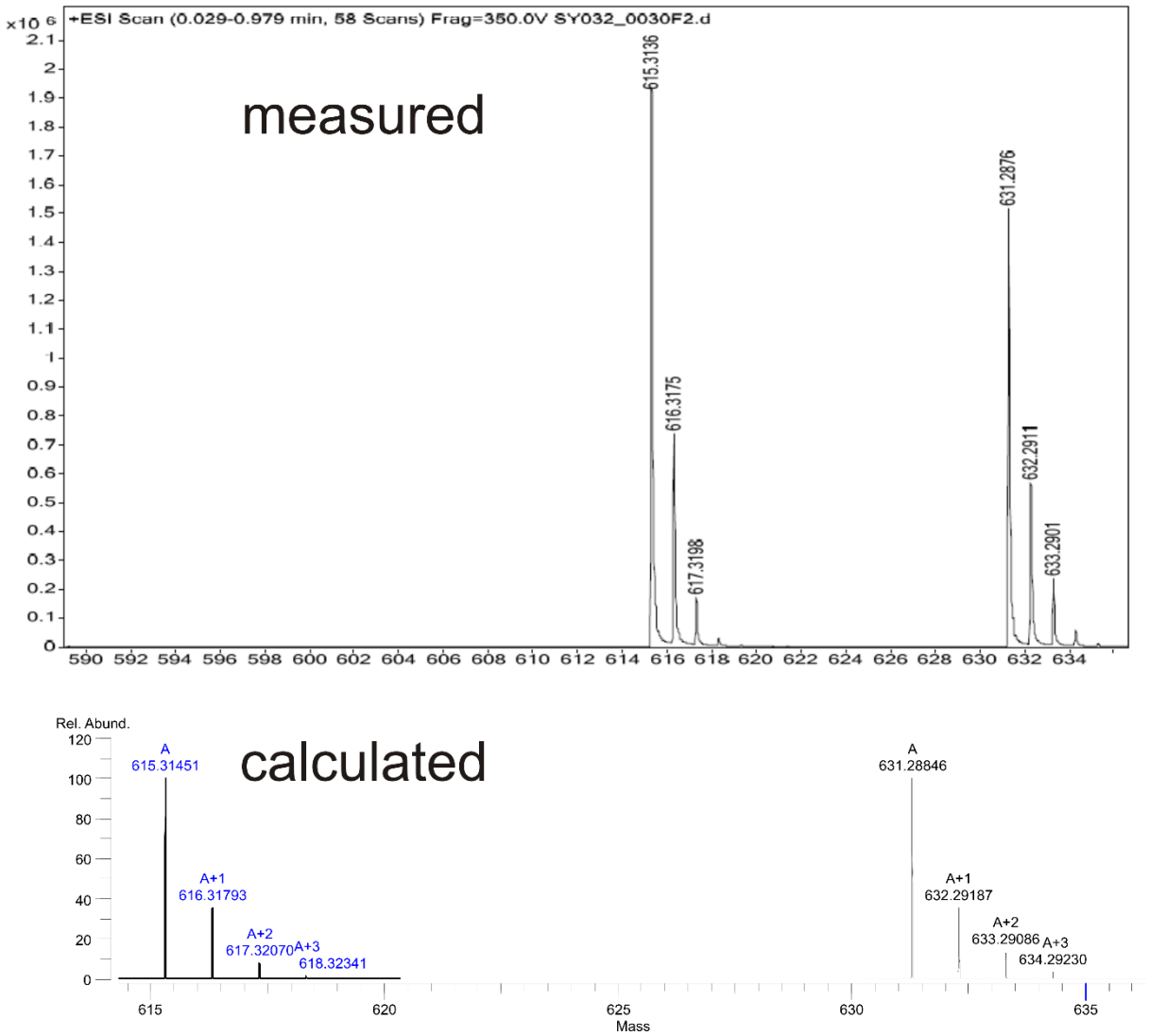

Fig. S37 HRMS ESI$^+$ (top) and calculated (bottom) of **S8**.

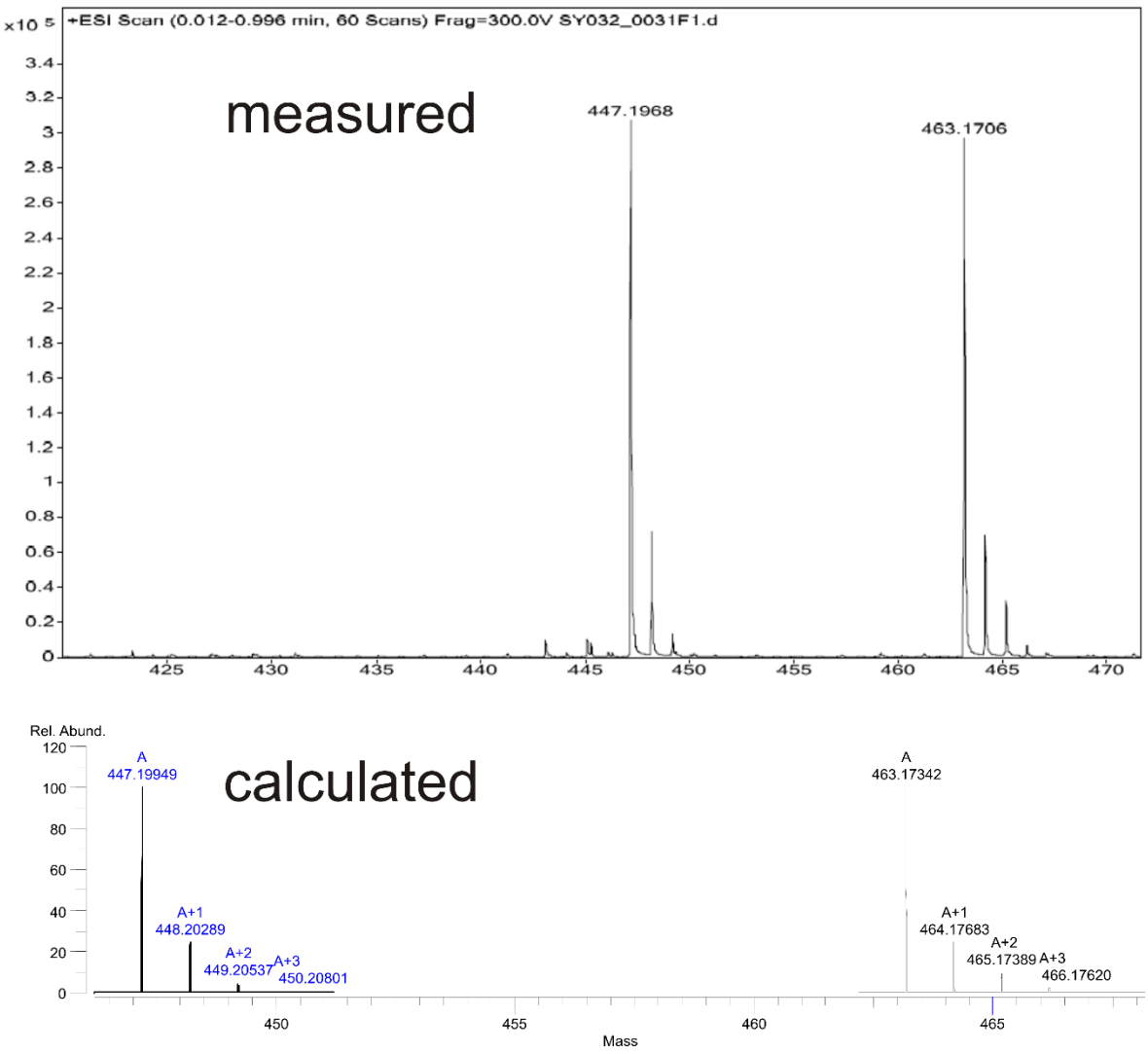

Fig. S38 HRMS ESI$^+$ (top) and calculated (bottom) of **S9**.

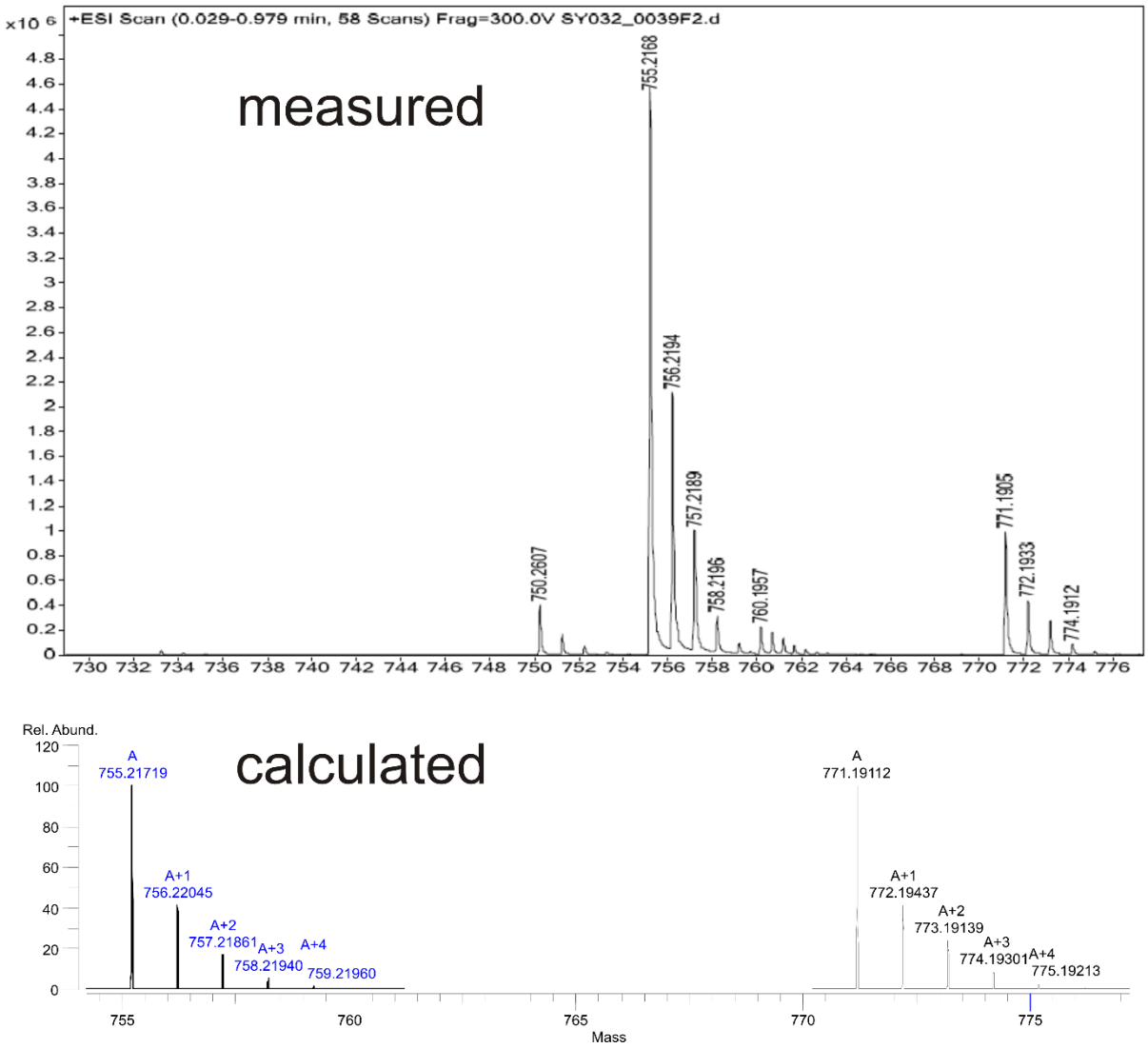

Fig. S39 HRMS ESI$^+$ (top) and calculated (bottom) of **S10**.

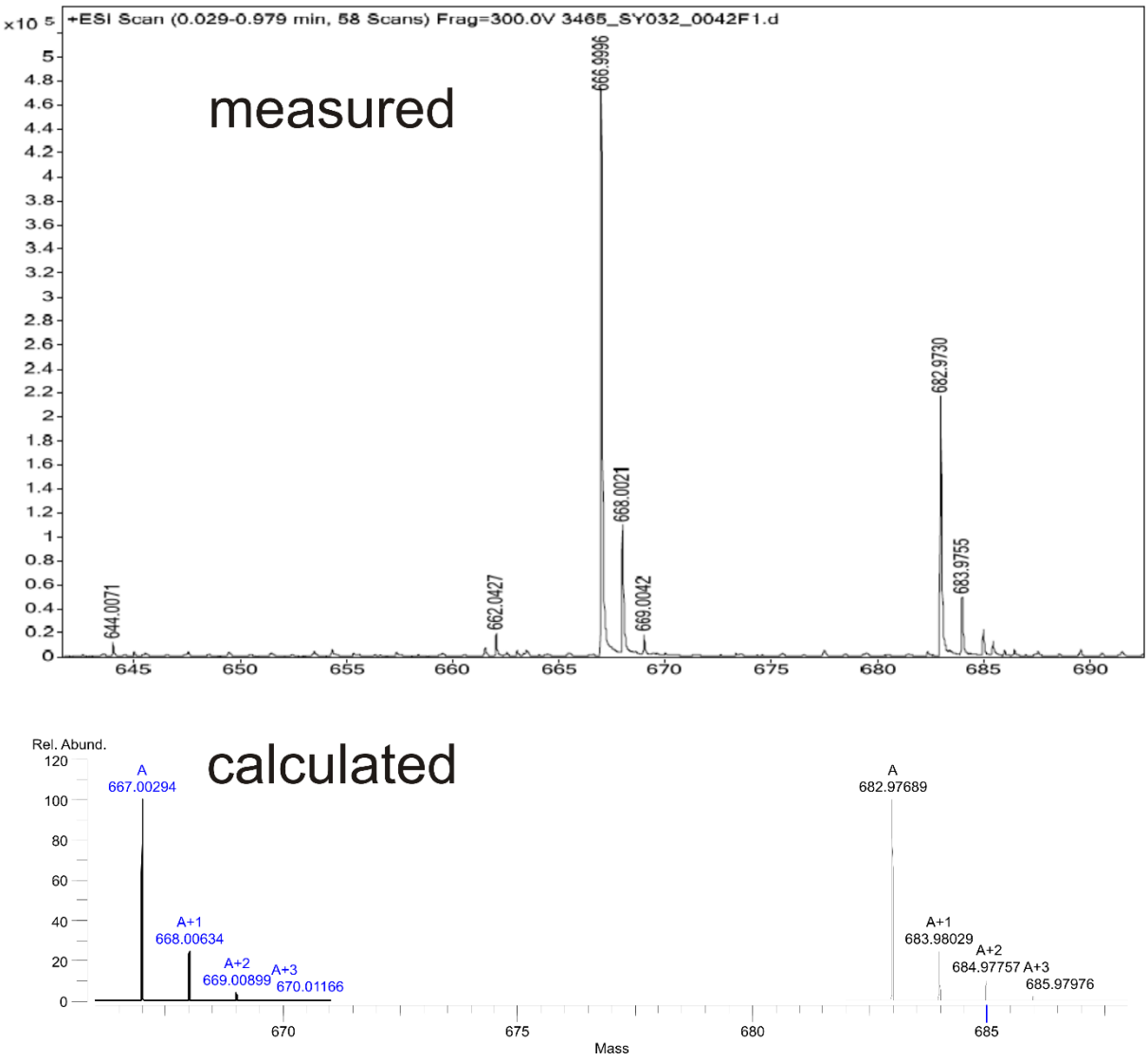

Fig. S40 HRMS ESI$^+$ (top) and calculated (bottom) of **S11**.

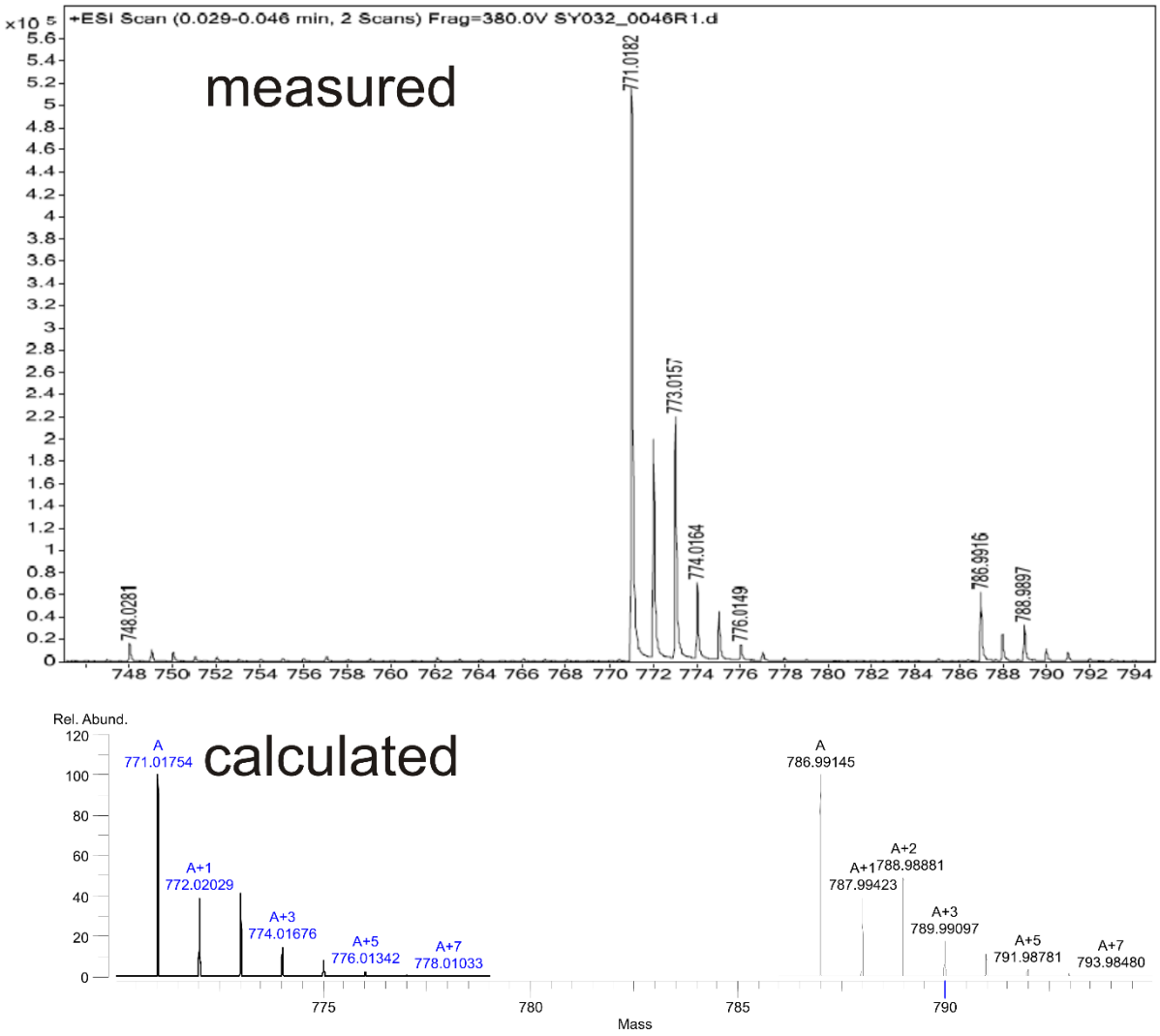

Fig. S41 HRMS ESI$^+$ (top) and calculated (bottom) of **dTTFC8**.

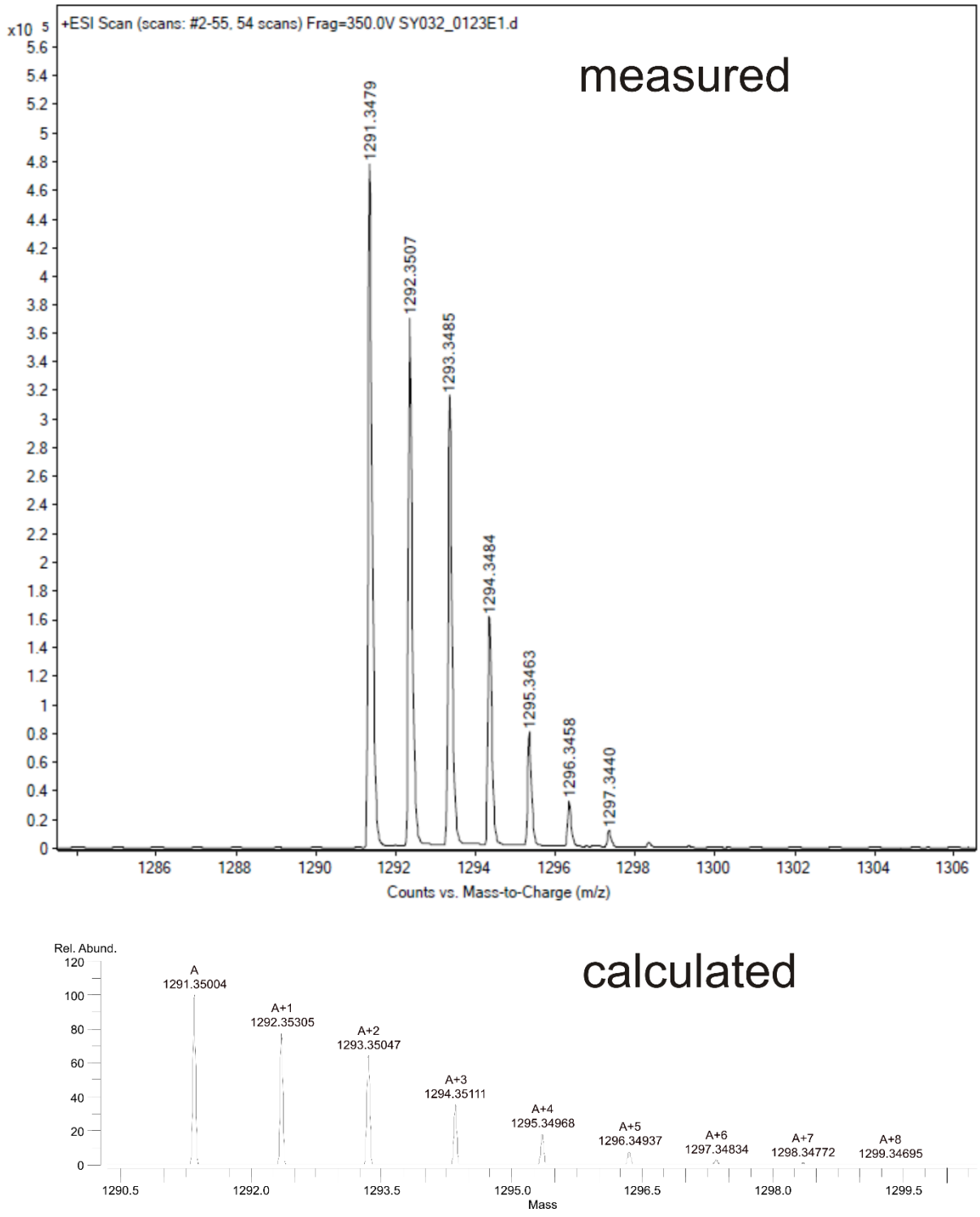

Fig. S42 HRMS ESI$^+$ (top) and calculated (bottom) of (*rac*)-**2**.

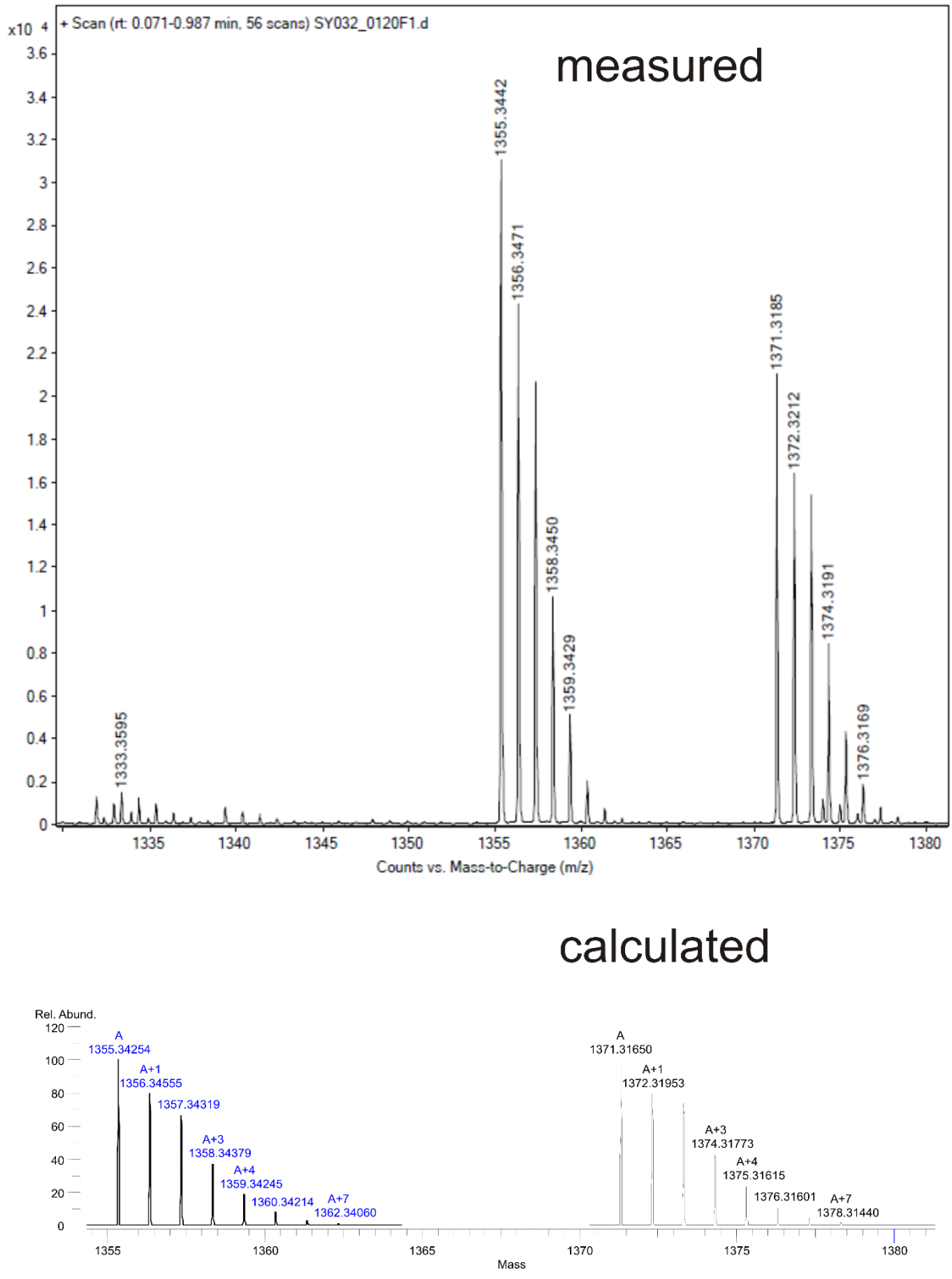

Fig. S43 HRMS ESI$^+$ (top) and calculated (bottom) of (*rac*)-**2Ac**.

11. References

1. M. Popr, S. Hybelbauerova and J. Jindrich, *Beilstein J. Org. Chem.*, 2014, **10**, 1390-1396.
2. W. Mamdouh, I. H. Uji, A. E. Dulcey, V. Percec, S. De Feyter and F. C. De Schryver, *Langmuir*, 2004, **20**, 7678-7685.
3. N. Svenstrup, K. M. Rasmussen, T. K. Hansen and J. Becher, *Synthesis*, 1994, **1994**, 809-812.
4. H. V. Schröder, S. Sobottka, M. Nößler, H. Hupatz, M. Gaedke, B. Sarkar and C. A. Schalley, *Chem. Sci.*, 2017, **8**, 6300-6306.
5. T. Matsumura, F. Ishiwari, Y. Koyama and T. Takata, *Org. Lett.*, 2010, **12**, 3828-3831.
6. J. R. Aranzaes, M.-C. Daniel and D. Astruc, *Can. J. Chem.*, 2006, **84**, 288-299.
7. X. Z. Zhu and C. F. Chen, *J. Am. Chem. Soc.*, 2005, **127**, 13158-13159.
8. K. Zimmermann, *Synth. Commun.*, 1995, **25**, 2959-2962.
9. S. Passemard, D. Staedler, L. Ucnova, G. S. Schneiter, P. Kong, L. Bonacina, L. Juillerat-Jeanneret and S. Gerber-Lemaire, *Bioorg. Med. Chem. Lett.*, 2013, **23**, 5006-5010.
10. J. Sly, P. Kasak, E. Gomar-Nadal, C. Rovira, L. Gorriz, P. Thordarson, D. B. Amabilino, A. E. Rowan and R. J. Nolte, *Chem. Commun.*, 2005, **10**, 1255-1257.
11. K. B. Simonsen, N. Svenstrup, J. Lau, O. Simonsen, P. Mørk, G. J. Kristensen and J. Becher, *Synthesis*, 1996, **1996**, 407-418.
12. F. A. Loiseau, K. K. Hii and A. M. Hill, *J. Org. Chem.*, 2004, **69**, 639-647.
13. S. Grimme, C. Bannwarth and P. Shushkov, *J. Chem. Theory. Comput.*, 2017, **13**, 1989-2009.
14. D. Porezag, T. Frauenheim, T. Köhler, G. Seifert and R. Kaschner, *Phys. Rev. B*, 1995, **51**, 12947-12957.
15. *Grimme et. al.*
16. H. J. C. Berendsen, J. P. M. Postma, W. F. van Gunsteren, A. DiNola and J. R. Haak, *J. Chem. Phys.*, 1984, **81**, 3684-3690.
17. J.-P. Ryckaert, G. Ciccotti and H. J. C. Berendsen, *J. Comput. Phys.*, 1977, **23**, 327-341.
18. K. Eichkorn, O. Treutler, H. Öhm, M. Häser and R. Ahlrichs, *Chem. Phys. Lett.*, 1995, **240**, 283-290.
19. J. Tao, J. P. Perdew, V. N. Staroverov and G. E. Scuseria, *Phys. Rev. Lett.*, 2003, **91**, 146401.
20. S. Grimme, J. Antony, S. Ehrlich and H. Krieg, *J. Chem. Phys.*, 2010, **132**, 154104.
21. S. Grimme, S. Ehrlich and L. Goerigk, *J. Comput. Chem.*, 2011, **32**, 1456-1465.
22. F. Weigend and R. Ahlrichs, *Phys. Chem. Chem. Phys.*, 2005, **7**, 3297-3305.
23. R. Ahlrichs, M. Bär, M. Häser, H. Horn and C. Kölmel, *Chem. Phys. Lett.*, 1989, **162**, 165-169.
24. A. Klamt and G. Schüürmann, *Perkin Trans. 2*, 1993, **5**, 799-805.
25. F. Neese, F. Wennmohs, A. Hansen and U. Becker, *Chem. Phys.*, 2009, **356**, 98-109.
26. J. D. Chai and M. Head-Gordon, *J. Chem. Phys.*, 2008, **128**, 084106.
27. V. Barone and M. Cossi, *J. Phys. Chem. A*, 1998, **102**, 1995-2001.
28. F. Neese, *Wiley Interdiscip. Rev.-Comput. Mol. Sci.*, 2012, **2**, 73-78.
29. C. Bannwarth and S. Grimme, *Comput. Theor. Chem.*, 2014, **1040-1041**, 45-53.
30. J. P. Perdew, M. Ernzerhof and K. Burke, *J. Chem. Phys.*, 1996, **105**, 9982-9985.
31. T. Yanai, D. P. Tew and N. C. Handy, *Chem. Phys. Lett.*, 2004, **393**, 51-57.
32. Y. Zhao and D. G. Truhlar, *Theor. Chem. Acc.*, 2007, **120**, 215-241.
33. R. F. W. Bader, *Chem. Rev.*, 1991, **91**, 893-928.
34. T. Lu and F. Chen, *J. Comput. Chem.*, 2012, **33**, 580-592.
35. COLLECT, Bruker AXS, Inc., Madison, Wisconsin, USA, 2008.
36. Z. O. a. W. Minor, *Methods Enzymol., vol. 276, Macromolecular Crystallography, Part A,* , Academic Press, New York, 1997.
37. G. M. Sheldrick, *SADABS*. University of Göttingen, Germany, **1996**.
38. G. M. Sheldrick, *Acta Crystallogr., Sect. A: Found. Adv.*, 2015, **71**, 3-8.
39. G. M. Sheldrick, *Acta Crystallogr., Sect. C: Struct. Chem.*, 2015, **71**, 3-8.
40. A. L. Spek, *Acta Crystallogr., Sect. C: Struct. Chem.*, 2015, **71**, 9-18.

41. A. L. Spek, *Acta Crystallogr., Sect. D: Biol. Crystallogr.*, 2009, **65**, 148-155.
42. J. Sun, X. Lu, J. Shao, X. Li, S. Zhang, B. Wang, J. Zhao, Y. Shao, R. Fang, Z. Wang, W. Yu and X. Shao, *Chem. Eur. J.*, 2013, **19**, 12517-12525.
43. H. Kobayashi, R. Kato, T. Mori, A. Kobayashi, Y. Sasaki, G. Saito, T. Enoki and H. Inokuchi, *Mol. Cryst. Liq. Cryst.*, 2011, **107**, 33-43.
44. P. R. Ashton, J. Becher, M. C. T. Fyfe, M. B. Nielsen, J. F. Stoddart, A. J. P. White and D. J. Williams, *Tetrahedron*, 2001, **57**, 947-956.